STUDY OF A PLATINUM/GRAPHENE NANOFLAKES CATALYST FOR OXYGEN REDUCTION REACTION OF POLYMER ELECTROLYTE MEMBRANE FUEL CELLS

Md Mahdi Salehin Feroze

Department of Chemical Engineering

McGill University

Montreal, QC, Canada

February 2019

A thesis submitted to McGill University in partial fulfillment of the requirements of the degree of Master of Engineering

I dedicate this thesis to my amazing Nanavai (maternal grandfather), Mohammad Siddiqur Rahman, who left us on February 6, 2018.

“Always pass on what you have learned.”

- Yoda

ABSTRACT

This master's thesis investigates the electrocatalytic performance of graphene nanoflakes (GNF) as the support of a noble catalyst towards oxygen reduction reaction (ORR) in acidic medium for application in polymer electrolyte membrane fuel cells (PEMFC). The graphene nanoflakes support is synthesized using methods developed by Pristavita *et al.* in 2011. Introducing platinum onto the support using thermal plasma is shown not possible in part due to limitations arising from the high boiling point of platinum. A wet chemistry technique developed by Jaoun *et al.* in 2003 is used to successfully introduce platinum onto the GNF support. The synthesized catalyst shows superior electrocatalytic activity towards ORR compared to a noble commercial catalyst having carbon black as supports, these tests being performed at high rotation speeds of rotating disk electrode (RDE) tests.

RÉSUMÉ

Cette thèse portait sur les performances électrocatalytiques de nanoflocons de graphène (GNF) en tant que support d’un catalyseur noble pour la réaction de réduction de l’oxygène (ORR) en milieu acide pour application dans les piles à combustible à membrane électrolytique polymèriques (PEMFC). Le support de nanoflocons de graphène a été généré selon la méthode par plasma thermique développée par Pristavita *et al*. en 2011. L'addition de platine sur le support carboné à l'aide d'un plasma thermique n'a pas été possible en raison des limitations en particulier liées au point d'ébullition élevé du platine et au coûts élevés d'un tel précurseur dans un plasma thermique. La méthode chimique en phase liquide mise au point par Jaoun *et al.* en 2003 a été utilisé avec succès pour générer des nanoparticules de platine sur le support GNF. Le catalyseur ainsi formé a montré une activité électrocatalytique supérieure vis-à-vis de l'ORR par rapport à un catalyseur commercial noble supporté par des particules de noir de carbone, ceci étant évalué à des vitesses de rotation élevées lors d'essais à l'électrode à disque rotatif (RDE).

ACKNOWLEDGEMENTS

I am grateful to my creator, Allah for the privileged life He has bestowed upon me and the scientific wonders I have been able to witness.

I would like to thank my supervisor, Professor Jean-Luc Meunier for his guidance. I always enjoyed our conversations on scientific possibilities. I learned to work independently and trust my judgement because of him.

Family is very important to me. Without my parents, especially my mother, I would not be here today. My whole life is built on my mother's limitless sacrifice. I want to thank my elder sister for being my inspiration since childhood. A special thanks to the love of my life, my dearest wife Chandni for supporting me during my undergraduate and graduate studies.

I have met some wonderful friends and colleagues in the past few years. To Pierre and Ulrich, thank you for being my mentor and helping me in academia and real life with advice. To Aqeel and Deepak, thank you for deep conversations on life. I am grateful to all my friends especially Brian, Dibbya, Gabriel, Tanveer and Xin for making me a better person.

McGill's chemical engineering department has become my second home. I am in indebted to Frank for championing safety, and to Andrew, Anna, Gerald, Jo-Ann, Lisa, Lou, Louise, Ranjan for being there always when I needed them. The imaging in this thesis was done by two amazing people: Dr David Liu and Stéphanie Bessette. I am also grateful to Dr Chilian and Darren from the SLOWPOKE laboratory of Polytechnique for helping me with neutron activation analysis.

This research would not have been possible without financial support from the Faculty of Engineering of McGill University and Natural Science and Engineering Research Council of Canada (NSERC).

TABLE OF CONTENTS

LIST OF FIGURES

LIST OF TABLES

NOMENCLATURE

° : Arcdegree

%: Percent

µL: Microliter

Ag/AgCl : Silver/silver chloride

cm: Centimeter

CNT: Carbon Nanotube

DC : Direct Current

EDX: Energy Dispersive X-ray Spectroscopy

eV: Electron Volts

g: gram

GNF: Graphene nanoflakes

H_2SO_4: Sulphuric acid

ICP: Inductively Coupled Plasma

K: Kelvin

kPa: Kilopascal

kW: Kilowatt

mA: Milliamps

mg: Milligram

MHz: Megahertz

NAA: Neutron Activation Analysis

ORR: Oxygen Reduction Reaction

PEMFC: Polymer Electrolyte Membrane Fuel Cell

RDE : Rotating Disk Electrode

RF : Radio Frequency

RHE : Reverse Hydrogen Electrode

rpm: Revolutions per minute

SEM : Scanning Electron Microscopy

slpm: Standard liters per minute

SWNT : Single Wall Carbon Nanotube

TEM : Transmission Electron Microscopy

wt%: weight percentage

CHAPTER 1: INTRODUCTION

1.1 Problem definition

Polymer electrolyte membrane fuel cells (PEMFC) were first developed in the 1960s to help NASA run their first manned space vehicle [1]. Due to a water management issue in the electrolyte, NASA preferred alkaline fuel cells over PEMFCs later in the 70s. In early 1990s, interest around PEMFC got more traction and companies like Ballard Power Systems of Vancouver, Canada brought about a renaissance [2] that resulted in PEMFC being considered for a wide variety of applications: from delivering a few watts for mobile phones [3] and computers [4] to providing hundreds of kilowatt for buses [5] and industrial combined heat and power (CHP) systems [6]. The automotive industry is currently trying to make PEMFC a viable power source for fuel cell electric vehicles (FCEVs) which are possible long-term and sustainable solution to satisfy the demand for global mobility as an alternative to fossil fuel powered vehicles [7].

Using PEMFCs to power FCEVs commercially in a reliable, efficient and cost-effective way is challenging. The main two challenges are associated with the performance of FCEVs compared to conventional internal combustion engine (ICE) vehicles and establishment of a global hydrogen fueling station network. There is a gradual increase in the number of hydrogen fueling stations all over the world especially in North America and Europe [8]. According to the fuel cell technical team of the United States Department of Energy (DoE), the key challenge regarding performance of FCEVs is to decrease cost and increase power density of PEMFC systems while simultaneously working towards more durability [9]. Among the various components used inside a PEMFC stack, the catalyst accounts for 41% of the total system cost ($/kW) at a high production volume of 500,000 systems per year [10]. This significant cost arises due to the use of platinum group metal (PGM) as the standard catalyst used in PEMFC systems. The US DoE has set a target of 0.125 g PGM/rated kW inside a PEMFC system for the year 2020 in order to lower the cost [11].

To tackle the high cost and limited supply of PGM catalysts, scientific community has been conducting intensive research since the early 2000s to replace PGM by introducing nitrogen and other non-noble metal like Fe [12], Co [13], Mo [14], Ni [15] etc. to the carbon matrix of the catalyst. While there has been significant progress in terms of performance, no non-noble metal has been able to replace PGM commercially due to the inherent superior catalytic activity of the latter in an electrochemical setting. This thesis explores a different approach to solve the same problem by using graphene nanoflakes (GNF) as the carbon support in stead of carbon black, which is the industry standard, to synthesize a platinum-based catalyst. The purity and strong crystalline structure of the GNF have shown an improvement in stability of the oxygen reduction reaction (ORR) in PEMFC environment in the past. GNF and nitrogen-functionalized GNF also showed to influence the catalytic reaction, while it is expected to help in the transport of ions in solution and in the electronic conductivity [16]. The combined Pt/GNF structures may thus influence the overall electrical and mass transport within the PEMFC membrane layer in a way to optimize the overall activity of the PEMFC.

Graphene nanoflakes are nanoparticles of stacked graphene exhibiting a crystalline structure with a flake-like morphology, as first developed using thermal plasma by Pristavita *et al.* in the Plasma Processing Laboratory of McGill University [17]. Oxygen [18], nitrogen [19], sulphur [20] and iron [21] functionalities have been introduced to GNF support in the past using thermal plasma. This thesis continues the work by introducing platinum to the GNF support and synthesizes a noble catalyst for the oxygen reduction reaction of PEMFCs allowing a comparison to be drawn between GNF and carbon black as support of PEMFC catalysts.

1.2 Objectives

The focal point of this master's project is to introduce platinum nanoparticles onto a graphene nanoflakes support, prepare a catalyst for the oxygen reduction reaction in polymer electrolyte membrane fuel cells (PEMFCs), and test the activity of this catalyst through electrochemical characterization. The specific objectives of this thesis are the following:

1) Determine a convenient method to introduce platinum nanoparticles to a graphene nanoflakes support.
2) Investigate the structure and composition of the platinum nanoparticle within the graphene nanoflakes framework.
3) Validate the electrocatalytic performance of the synthesized catalyst towards oxygen reduction reaction (ORR) in an acidic environment against an industry standard catalyst with similar platinum composition.

The methodology to acquire these objectives includes identifying an appropriate platinum precursor.

1.3 Organization of the thesis

There are 5 chapters in this thesis. Chapter 2 provides a literature review on PEMFCs, the various challenges associated with its operation and the history of various carbon supports used over the years to synthesize fuel cell catalysts. The methodology used to carry out the experiments and the techniques used to synthesize and characterize the platinum/graphene nanoflake catalyst are outlined in Chapter 3. Chapter 4 focuses on the discussion of the main results obtained over the course of this master's research project. The final chapter presents concluding remarks based on the findings and proposes some recommendations for future work.

CHAPTER 2: BACKGROUND & LITERATURE REVIEW

2.1 Fuel cells

Heat engines such as steam turbines and internal combustion engines (ICE) produce mechanical energy by converting thermal energy through a Carnot cycle that obeys the Second Law of Thermodynamics. During this conversion a significant portion of thermal energy is irretrievably lost. Fuel cells convert the energy of a chemical reaction directly to electrical energy through an electrochemical mechanism without passing through thermal and mechanical energy forms. This working principle allows fuel cells to avoid any significant energy loss during energy conversion making them inherently more efficient compared to any traditional heat engine [22]. The efficiency of the most efficient 4-stroke diesel engine in the world is around 50% [23] whereas high temperature fuel cells like solid oxide fuel cell can easily reach an efficiency of 60% while the theoretical limit is above 80% [24].

At the end of the nineteenth century, grid power started to replace galvanic cells and storage batteries in laboratories and homes due to emergence of electric generator in 1864. A German physical chemist, Wilhelm Ostwald came up with the idea of using electrochemical mechanism instead of combustion of natural fuel used in thermal power plants realizing the intermediate stage of heat generation is being bypassed. Even though British scientist Sir William Grove and German scientist Christian Friedrich Schoenbein were the ones to build the first fuel cell, it was Wilhelm Ostwald who pioneered the general theory of fuel cells first [25].

There are two metal electrodes dipped in an electrolyte solution in a simple fuel cell as shown in Figure 1. While in operation, electrons are produced at the anode through oxidization of a fuel and the cathode absorbs those electrons through reduction of an oxidizing agent. Continuous supply of reactant fuel and withdrawal of reaction products from the electrodes is essential to keep the fuel cell operating.

Working voltage of an individual fuel cell is lower than the theoretical thermodynamic electromotive force due to internal ohmic resistance and electrode polarization that happens due to a shift of potential of the electrodes when the current starts to flow. For real life applications, appropriate number of fuel cells are connected in series forming a stack to meet the voltage demand.

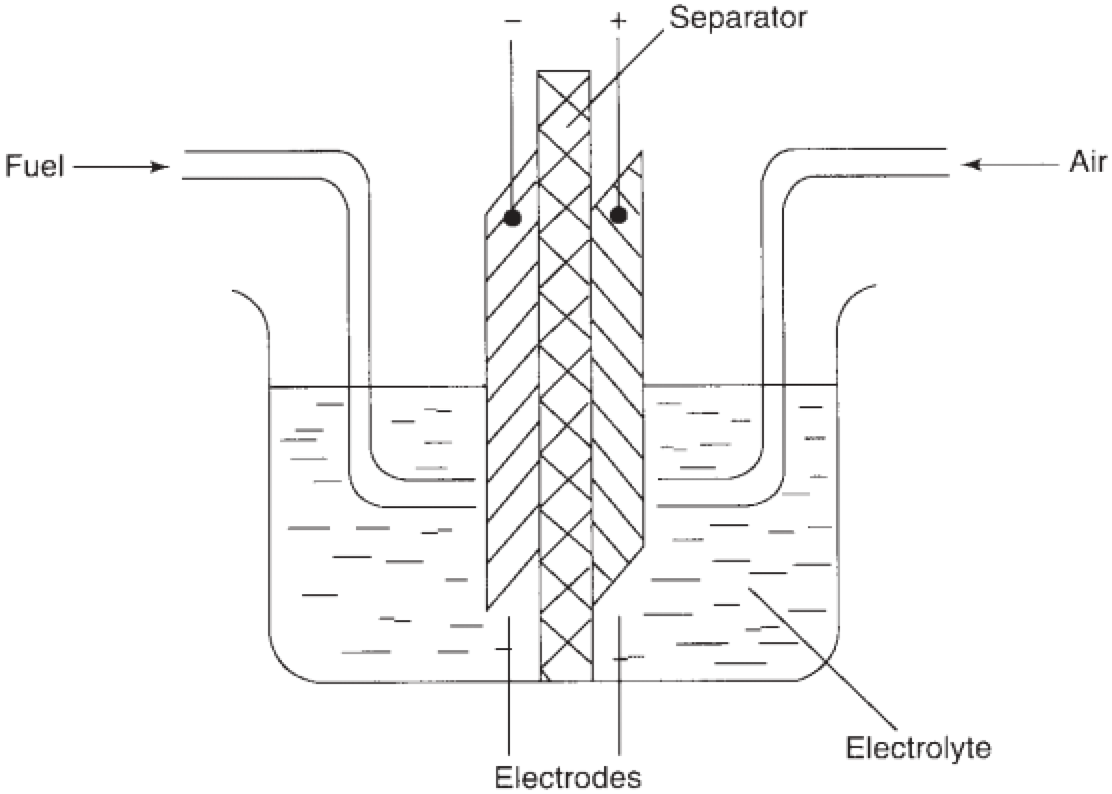

Figure 1: Schematic of an individual fuel cell [22].

Fuel cells can be differentiated based on attributes like reactant type, electrolyte type and working temperature [24]. Key characteristics of the main fuel cell types are presented in Table 1

Table 1: Key attributes of different fuel cell types

Attribute Name	**Polymer Electrolyte Membrane Fuel Cells (PEMFC)**	**Alkaline Fuel Cells (AFC)**	**Phosphoric Acid Fuel Cell (PAFC)**	**Molten Carbonate Fuel Cell (MCFC)**	**Solid oxide Fuel Cell (SOFC)**
Electrolyte	Hydrated polymeric ion exchange membranes	Mobilized or immobilized potassium hydroxide in asbestos matrix	Immobilized liquid phosphoric acid in SiC	Immobilized liquid molten carbonate in $LiAlO_2$	Perovskites (Ceramics)
Electrodes	Carbon	Transition metals	Carbon	Nickel and Nickel Oxide	Perovskite and perovskite/metal cermet
Catalyst	Platinum	Platinum	Platinum	Electrode Material	Electrode Material
Operating Temperature	40 – 80°C	65 – 220°C	205°C	650°C	600 – 1000°C
Charge Carrier	H^+	OH^-	H^+	CO_3^{2-}	O^{2-}

2.2 Polymer electrolyte membrane fuel cells (PEMFCs)

In a polymer electrolyte membrane fuel cell, a polymer membrane serves as a solid electrolyte and exchanges proton between the electrodes. The conductivity of the membrane results from continuous hydration that leads to dissociation of acidic functional groups and formation of protons that move freely throughout the membrane.

A single PEMFC is shown below in Figure 2. PEMFCs use hydrogen and oxygen as reactants. Considering the method of proton exchange through the membrane facilitated by water molecules, the electrochemical reaction occurring at the electrodes of PEMFCs can be written as the following:

$$\mathrm{Anode: 2H_2 + 4nH_2O \ \rightarrow 4H^+.nH_2O + 4e^-}$$

$$\mathrm{Cathode: O_2 + 4H^+.nH_2O \ \rightarrow (n+2)H_2O}$$

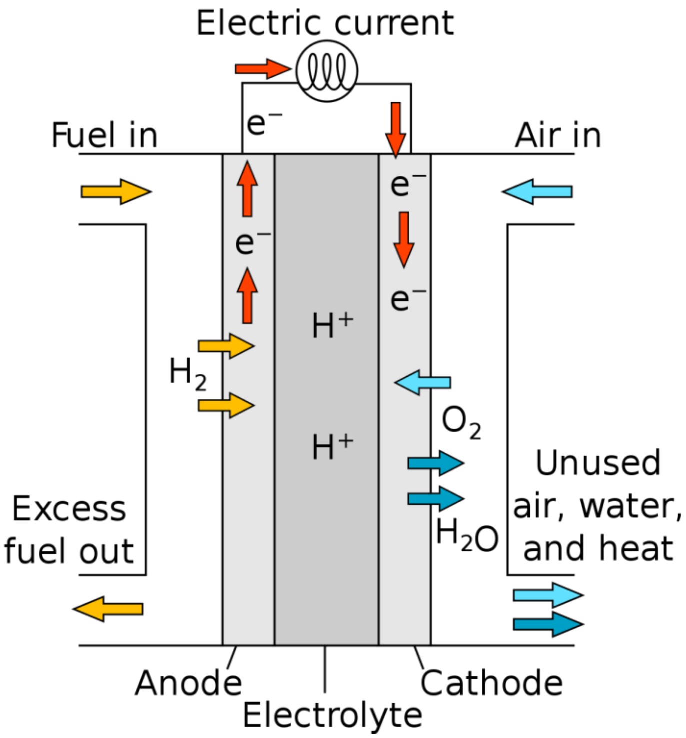

Figure 2: Individual proton exchange membrane fuel cell [26].

The first version of PEMFC was built by General Electric in the 1960s for the Gemini spacecraft of NASA. The proton exchange membrane was made from sulfated polystyrene which served as the electrolyte. The cell boasted 1kW rated power, but the total lifetime was below 200 hours due to chemical instability. The platinum loading in the electrodes was around 4 mg/cm^2 which resulted in high cost for a single unit limiting the use to only space flight applications [27]. In the 1990s, the potential of PEMFC in zero emission cars received attention due in large part to notable improvements in the electrolyte membrane properties. Development of the Nafion proton-exchange membrane by DuPont, distinctive membrane-electrode assemblies (MEA) and optimum utilization of platinum in the electrodes played strong role in the advancement of this technology.

Nafion is a perfluorinated sulfonic acid polymer (PSAP) that has a continuous skeleton of $– (CF_2)_n –$ groups with several hydrophilic sulfonic acid groups ($– SO_3H$) attached to it. When nafion is wet, the sulfonic acid groups dissociate and provide high protonic membrane conductivity at 80^oC. This process controls the operating temperature of PEMFCs. The membranes need to be thin enough to have low ohmic resistance and thick enough to prevent occasional failure that may lead to mixing of gas inside a fuel cell. Over the years, scientists have been able to engineer a balanced structure and composition of nafion that contributed to improved performance of PEMFCs [28]. The structure of nafion is shown below in Figure 3.

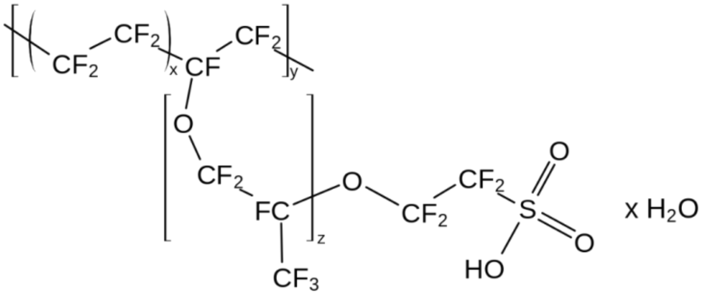

Figure 3: Structure of nafion [29].

The nafion membrane separating the two electrodes forms the membrane electrode assembly (MEA). The electrodes consist of a porous gas diffusion layer (GDL) with a thin layer of electrocatalyst named the catalyst layer (CL). The catalyst layer is responsible for driving the electrochemical reactions taking place at each electrode. The gas diffusion layer and the catalyst layer combinedly is called the gas diffusion electrode (GDE). In a single fuel cell, the MEA is situated between two current collector plates (CCP). These plates distribute the fuel and oxidant within the cell, facilitate management of water, separate different cells in a stack and carry the current away from the cell. The channels on the face of the plates can be serpentine or grid-like in nature. A fuel cell stack is formed by inserting the MEAs with bipolar plates machined on both faces between two end plates. The bipolar plates can be made from non-porous graphite, coated metal or metal/carbon based composite material [30]. A sample fuel cell stack is presented in Figure 4.

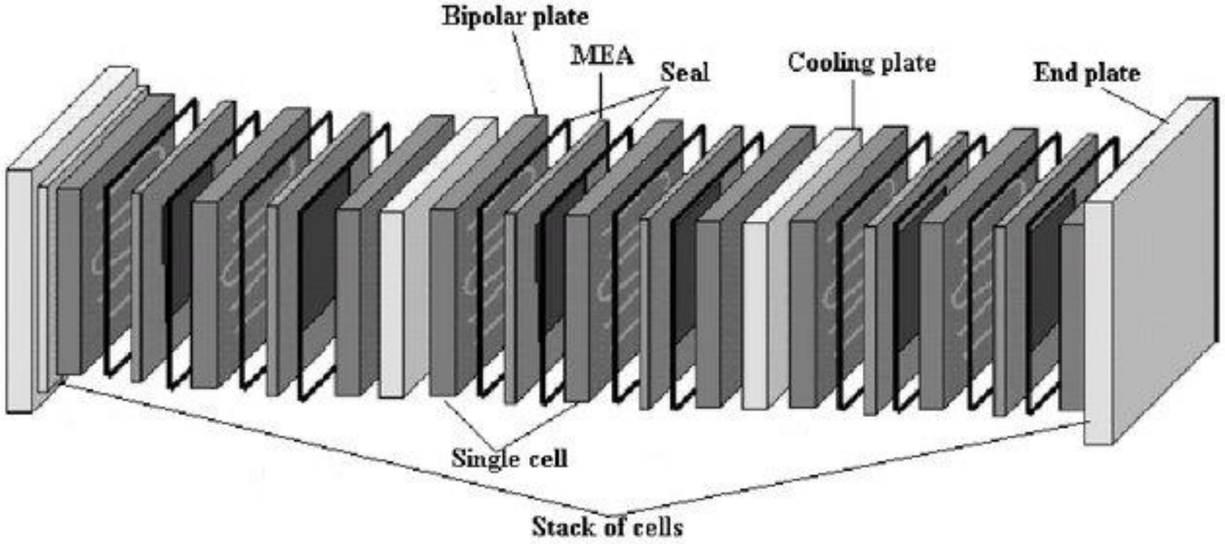

Figure 4: Components of a fuel cell stack [31].

In earlier stages of development, pure platinum was dispersed in the PEMFC electrodes directly resulting in a large amount of platinum being used. Depositing platinum onto highly dispersed carbon black support increased the specific surface area by more than 6 folds [22]. The catalytic activity of the platinum depends not only on the amount of platinum deposited on the support but also the method of deposition of the platinum onto the support [32]. Platinum is very susceptible to poisoning by carbon monoxide (CO) that maybe present in the hydrogen feedstock if syngas is used. A significant increase in electrode polarization can be observed due to the presence of even trace amounts of CO. Gottesfeld *et al.* reported an increase in anode polarization by 0.2 to 0.3 V for only 25 ppm CO present in the hydrogen feedstock leading to a loss of 30 to 40% electrical power [33]. Selective oxidation of CO by using current pulses [34] or operating PEMFCs at a temperature higher than 100^{o}C may solve the poisoning problem temporarily but promote other difficulties. The most reliable way to tackle the poisoning problem at the anode is to use mixture of platinum – ruthenium (Pt-Ru) as catalyst which is appreciably less sensitive towards CO poisoning compared to pure platinum [35].

The operating conditions of PEMFC must be chosen carefully to avoid additional problems that may arise from improper water management, excessive heat generation, higher partial pressure of the reactant gases and the influence of ambient temperature [22].

2.3 Carbon as catalyst support in PEMFCs

Carbon is the most abundant element inside a PEMFC. The polymer electrolyte membrane has a carbon backbone. Catalyst layer, gas diffusion layer and current collector plates are all made from graphitic carbon. The most significant use of carbon in a fuel cell is as the support of PGM catalyst. Carbon support enhances the performance of catalysts by influencing the shape, size and dispersion of the catalyst nanoparticles [36]. To achieve stabilization of PGM in a highly dispersed state, the underlying carbon support needs to be heterogenous in nature meaning the surface of the support needs to be a mixture of edges and basal planes [37].

Hegenberger *et al.* described a metal-active carbon interaction based on charge transfer from metal to the carbon support. According to the model, the charge transfer is approximately equal in value to the number of surface state in the energy gap of the carbon support's surface [38]. In graphitic surfaces, this leads to an increased mobility of transition metal atoms and formation of clusters due to difference between the cohesive energy of these metals and the adsorption enthalpy. Formation of nanoparticles on graphitic surfaces can be distinguished as diffusion limited aggregation where nucleation sites are chemically or structurally defected [39]. Nanostructured allotropes of carbon such as carbon nanotubes (CNT), carbon nanofibers (CNF), mesoporous carbon, nanodiamonds and graphene have high surface area, high electrical conductivity and relatively good stability in acid media. Among these CNT and CNF stand out for their higher graphitic nature and are reported to be more stable [40].

2.3.1 Carbon black

The most common carbon support of PGM catalysts in commercial fuel cells is Vulcan XC-72 which is a form of carbon black (CB). CB is generally synthesized by pyrolysis of hydrocarbons and consists of near-spherical particles of graphite that are typically <50 nm in diameter. CB is used extensively in research and in the fuel cell industry due to its high surface area (~250 m^2g^{-1}), wide availability and low cost.

Despite being the industry standard, CBs have limitations. Presence of organo-sulphur impurities and deep micropore or recesses that trap catalyst nanoparticles reducing their access to reactants lead to reduced catalytic activity. When the size of Nafion micelles (>40 nm) are larger than the recesses of CB, the accessibility of metal nanoparticles with lower diameter than the micelles is reduced significantly, and the nanoparticles do not contribute towards electrochemical activity. CBs also lack thermochemical stability in an acidic environment which is essential to prevent carbon corrosion. Carbon corrosion leads to disintegration of catalyst layers inside PEMFCs [41].

2.3.2 Carbon nanotubes (CNT)

CNTs are two dimensional rolled up single sheets carbon atoms that are arranged hexagonally. CNTs can be single walled (SWCNT) or multi-walled (MWCNT) as shown in Figure 5. Pristine CNTs are chemically inert but their surface can be functionalized with oxygen groups. Different methods like sputter disposition [42], ion-exchange [43] and electrochemical deposition [44] can be used to deposit metal nanoparticles on CNTs.

Park *et al.* investigated MWCNT supported platinum catalyst that exhibited higher corrosion resistance and stronger interaction with Pt nanoparticles compared to platinum supported on Vulcan XC-72. MWCNT prevented the catalyst layer on the cathode side from flooding by maintaining electrode structure for a long period of time while under continuous anodic potential stress [45].

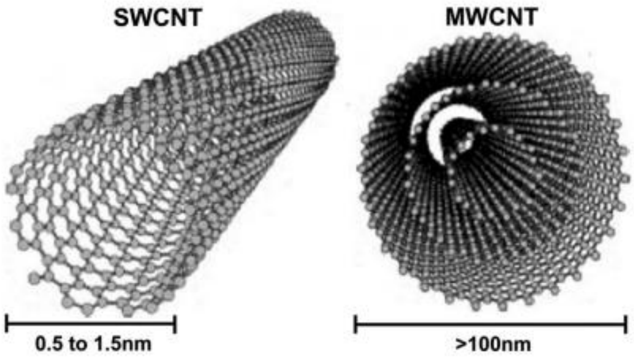

Figure 5: Schematic representation of SWCNT and MWCNT [46].

There are however cost problems associated with large scale production of CNTs. The cost of production has been reduced significantly in recent years, but further reduction is still required for CNTs to become viable commercially as a solution for the replacement of carbon black.

2.3.3 Carbon nanofiber

Carbon nanofibers (CNF) have very thin or no hollow cavity compared to CNTs as illustrated in Figure 6. Since they were first produced by the decomposition of hydrocarbons over metal particles, they have been extensively researched as catalyst support for fuel cells [47]. CNFs can be ribbon-like, platelet shaped or stacked-cup/herringbone depending on the orientation compared to the growth axis. Among the three different classes, herringbone CNFs have exhibited higher catalytic activity and better durability due to the intermediate nature of its structure compared to the other two classes [48].

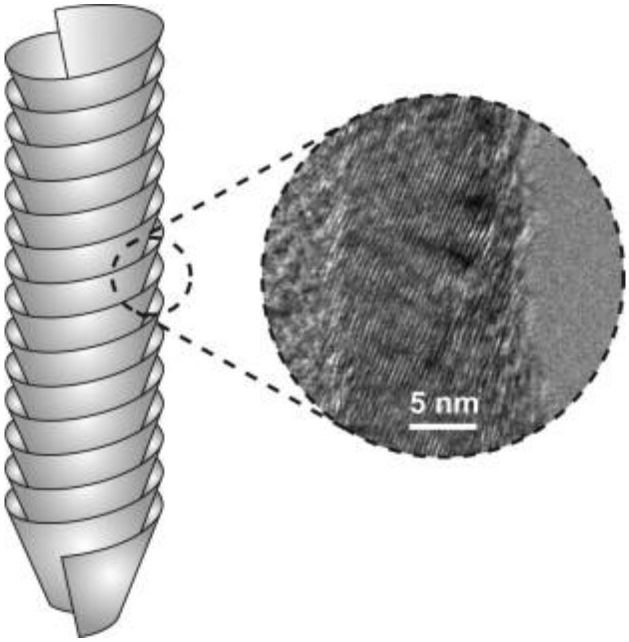

Figure 6: Schematic of carbon nanofiber structure with a TEM image exhibiting an inclined orientation of stacked graphene sheets with respect to the nanofiber axis [49].

Kang *et al.* performed durability studies on platinum-ruthenium catalyst supported by CNF for direct methanol fuel cells and achieved a constant current density of 150mAcm^{-2} for 2000 h [50].

2.3.4 Mesoporous carbon

Mesoporous carbon materials have pore sizes between 2-50 nm that provide high surface area and facilitate conductivity. They can be ordered (OMC) or disordered (DOMC) depending on the structure and preparation method. OMCs are prepared using mesoporous silica sieves as templates [51]. OMCs have been widely studied as catalyst support for fuel cells because of their high surface area and ability to facilitate diffusion of reactants and by-products utilizing the three dimensionally connected mono-dispersed mesospheres [52].

Liu *et al.* synthesized nitrogen doped ordered mesoporous graphitic arrays using nanocasting that resulted in a narrow pore-size distribution. A moderate nitrogen content provided high surface area, increased electrocatalytic activity and excellent stability compared to commercial platinum-carbon catalysts [53].

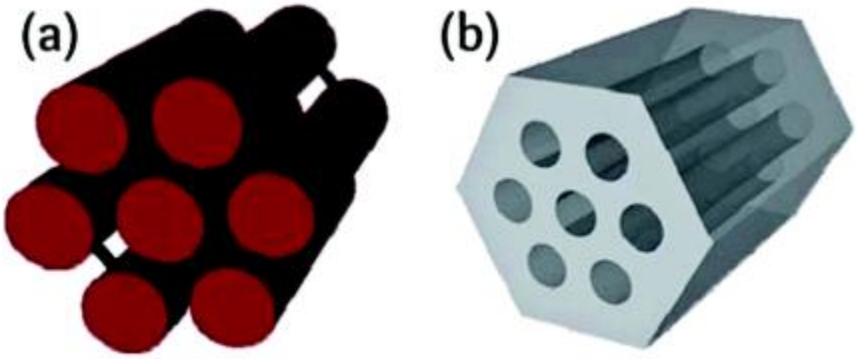

Figure 7: Schematic models of ordered mesoporous carbon [54].

2.3.5 Nanodiamonds and doped diamonds

Diamond is an insulator with a high band gap higher than 5 eV. Boron or phosphorus can be used as dopants to form p-type or n-type nanodiamonds. Boron is the most popular dopant due its low activation energy of 0.37 eV. Boron doped diamond (BDD) films can be a viable support for PEMFC catalyst because of its wide electrochemical potential, high electrochemical stability and corrosion resistance in both acidic medium [55]. In order to introduce platinum onto BDD support different methods have been used in the research community including thermal decomposition [56], implantation [57] and electrochemical deposition [58].

Lu *et al.* studied the role of BDD as a support for electrodeposited Pt-Ru alloy nanoparticles. Resulting electrodes exhibited high electrochemical activity and tolerance towards CO poisoning [59]. Using boron as a dopant increases the conductivity of diamonds but it can also affect the stability inversely [47].

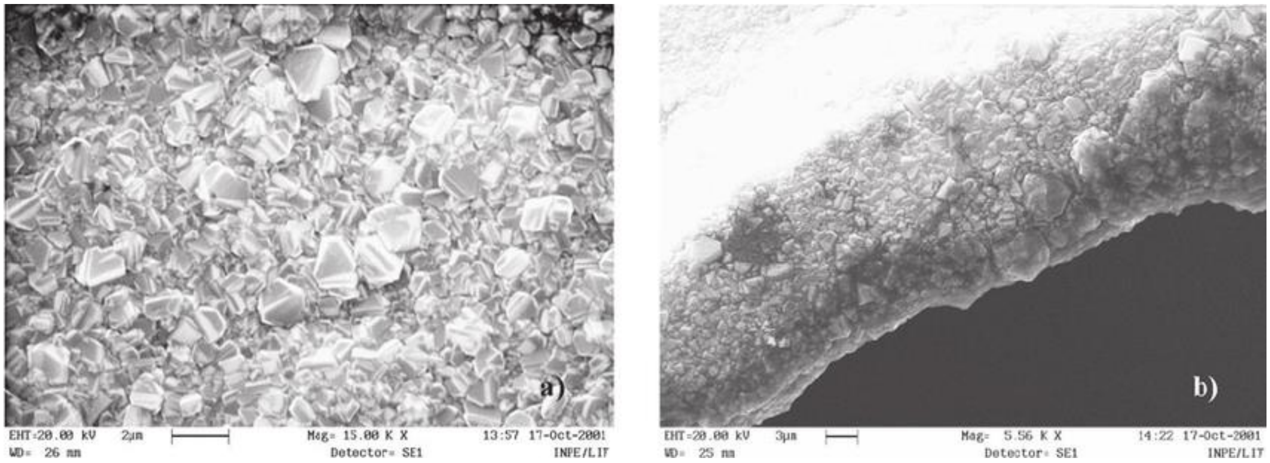

Figure 8: Scanning electron micrographs of boron-doped diamond film (a) superficial vision; (b) vision of the border of the sample [60].

2.3.6 Graphene

Graphene was first developed by Novoselov *et al*. Graphene is atomically thin sheet of carbon atoms arranged hexagonally and it offers high conductivity as well as electron transfer capabilities [61]. Graphene and its oxide have been widely studied for applications inside PEMFCs including their role as catalyst support [62], composite material with polyfluorinated polymer in polymer electrolyte membranes [63] and bipolar plate material [64].

Chu *et al.* investigated nitrogen doped three-dimensional graphene supported platinum catalysts for PEMFCs. The catalyst exhibited higher electrocatalytic activity towards oxygen reduction reaction and better stability after 1000 cycles compared to commercial platinum/carbon catalysts [65].

A variety of graphene material exist that can be separated into two main families based on their synthesis route being (a) the top-down approaches most often based on the exfoliation of graphitic materials using oxidation, and (b) the bottom up approaches based on building the graphene layers from the atomic level (CVD and the plasma-based approach used in the present thesis). Two important differences in these approaches is the level of defects in the structures and the amount of impurity, the bottom-up approach generally having much lower amounts of defects in the structure (higher crystallinity), and much higher purity. The graphene nanoflake (GNF) structure and synthesis used in this thesis will be described in more details in Section 3.1. The price and quality of mass-produced graphene using different methods is shown in Figure 9.

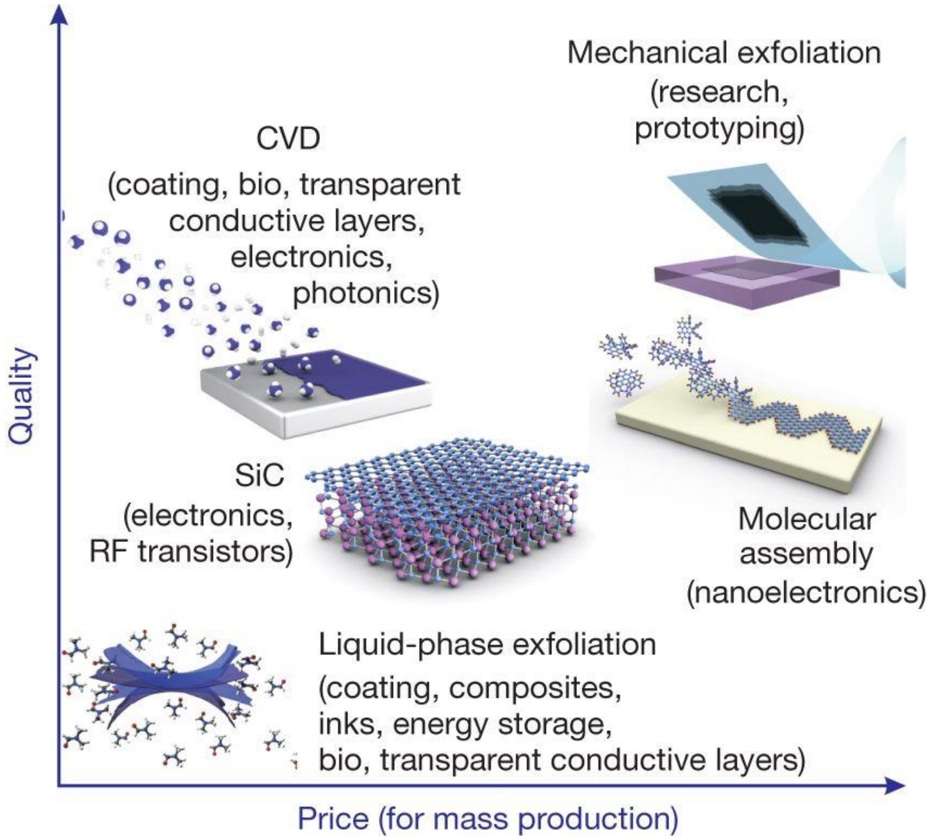

Figure 9: Methods of mass-production of graphene depending on applications [66]

2.4 Non-carbon material as catalyst support

Apart from carbonaceous materials, titanium oxide [67], silica [68], tungsten [69], and zirconia [70] have also been explored as potential supports for PEMFC catalysts due to their significantly higher resistance towards corrosion which is common among different supports in varying degrees. In the strong oxidative conditions inside a PEMFC, the inertness of non-carbon supports makes them less susceptible to any degradation. Moreover, Lewera *et al* observed a partial charge transfer from titanium oxide support to platinum that resulted in increased electron density and an enhanced electrocatalytic activity of the platinum support system towards oxygen reduction reaction [71].

3. RESEARCH METHODOLOGY

3.1 Pt/GNF growth in thermal plasma reactor

Graphene nanoflakes were grown using the procedure developed by Pristavita *et al.* which involves homogeneous nucleation of pure carbon material following the decomposition of a carbon precursor, namely methane, inside an inductively coupled plasma (ICP) system [17]. A procedure developed by Legrand *et al.* was then used to introduce platinum onto the GNF support by injecting a platinum nitrate salt solution directly into the thermal plasma [20].

The ICP system consists of a radio frequency (RF) generator, an ICP thermal plasma torch, a vacuum system, and a conical reactor. All these units are controlled from a central console that takes operating parameter inputs like pressure, gas flows, water flowrates and power. The thermal plasma generated by the ICP torch has a temperature in the order of 10,000 K. The diagram of the plasma torch body is presented in Figure 10.

The RF generator can provide up to 60 kW power with a frequency between 2 and 5 MHz to the plasma system. A separate cooling system provides 85 slpm of city water in a closed loop system in order to cool down the generator from excessive heating. The ICP torch used in this setup has a rated power of 35 kW. However, the power is not increased more than 25 kW during operation of the system. The body of the plasma torch consists of a ceramic confinement tube, induction coil, gas entrances, and a water-cooling system that provides the torch with 25 slpm water. The generation of plasma within the torch can be explained by principle of induction. Three to four turns of water-cooled copper coil wrap the ceramic confinement tube. When the generator delivers a RF current to the copper coil, an alternative magnetic field is induced that heats argon and create a thermal plasma. Continuous gas flow is required to sustain the plasma generated within the torch body.

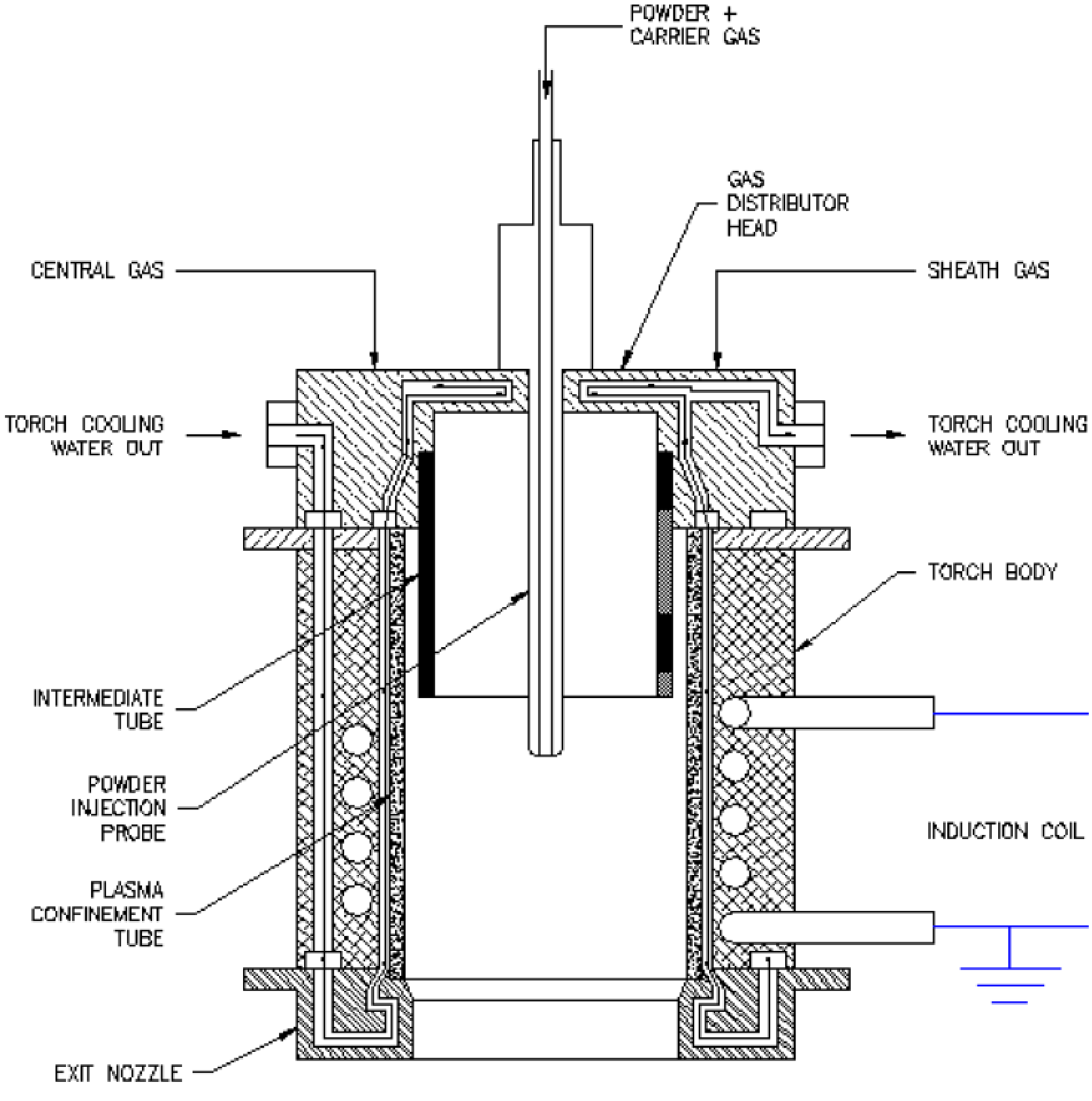

Figure 10: Schematic diagram of TEKNA's Induction Plasma Torch [72].

The conical water-cooled reactor is 50 cm long and has a full angle of expansion of 14^o as shown in Figure 11. Pristavita *et al.* customized the reactor and optimized the conical geometry of the reactor to allow gradual expansion of the gas and the conditions for the homogeneous nucleation of the carbon critical clusters.

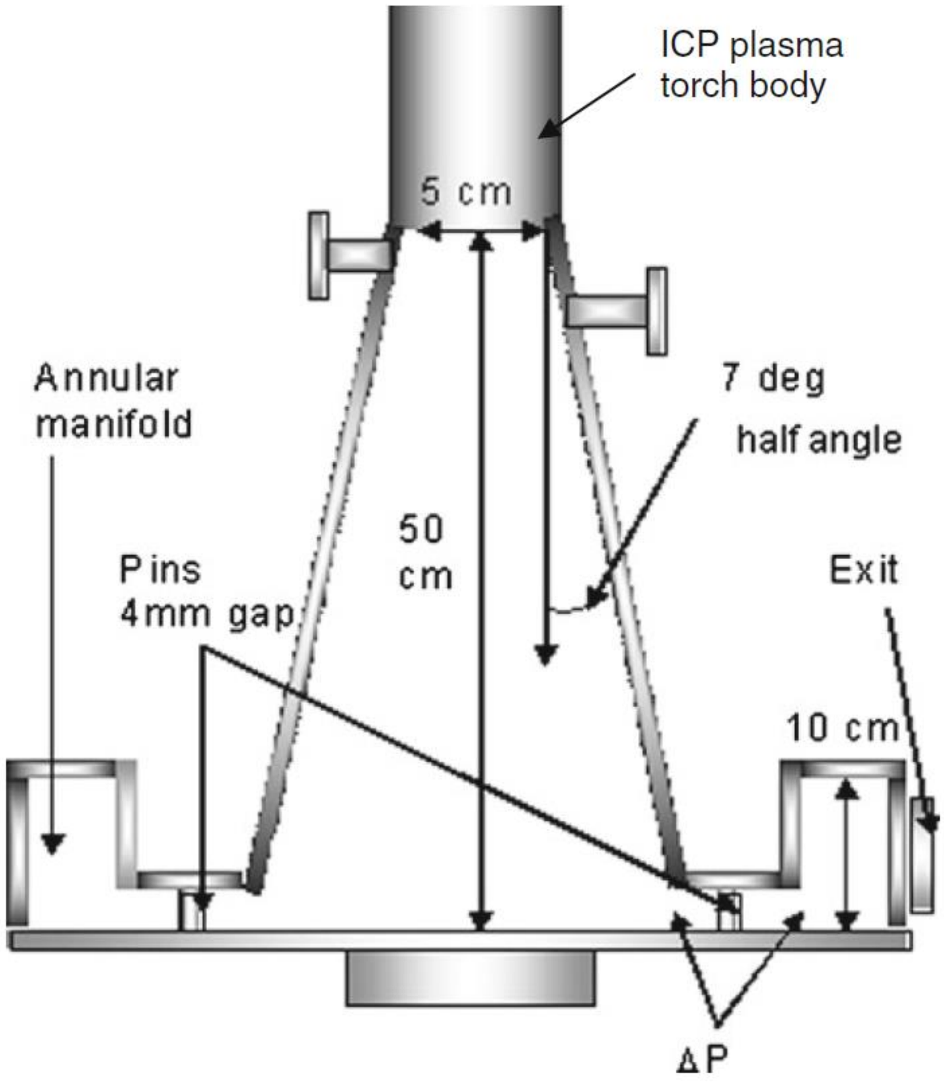

Figure 11: Diagram of conical; water-cooled reactor [73].

The temperature, flow velocity, and carbon density fields enable an increased residence time of these clusters in a growth zone and provide the 2-dimensional growth of the GNF structures. The gaseous precursors in the thermal plasma system being only argon and methane, the resulting GNF particles collected form a powder that is extremely pure as shown in Figure 12.

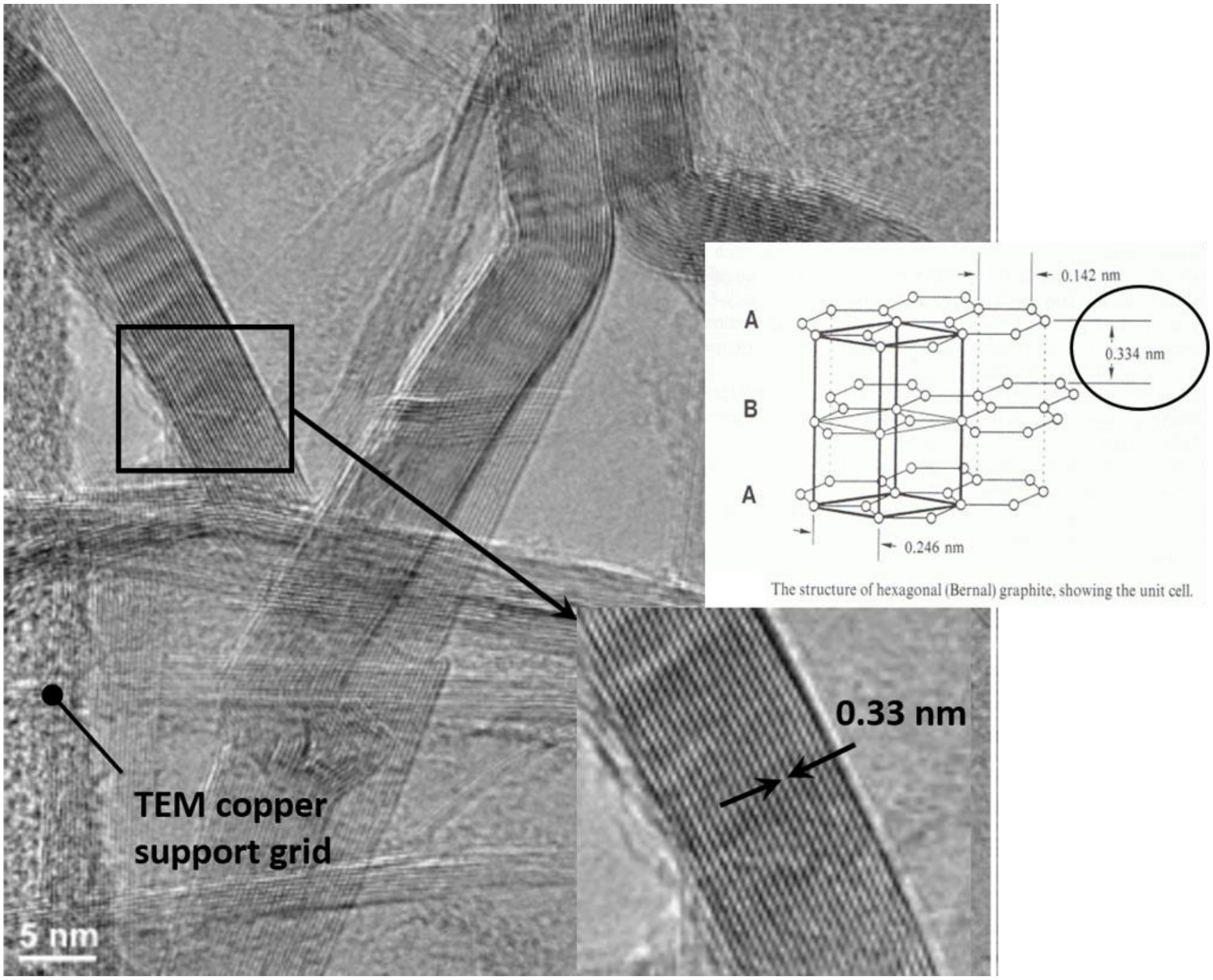

Figure 12: TEM imaging of GNF structure with the Bernal graphite structure inset for reference [74].

Such high purity is a strong asset in PEMFC operation, impurities being most often the cause of poor stability and catalyst degradation in fuel cell operation. The very high temperature of the GNF nucleation process also provides high mobility of the carbon atoms in the structure, and results in an extreme crystallinity of the GNFs [73]. Temperature, residence time, stream-function, particle diameter and other important parameters relevant towards pure GNF nucleation and growth inside the conical reactor were modeled by Meunier *et al.* [75]. Legrand *et al.* optimized the pressure, power, and flowrate while functionalizing the GNF support using a liquid precursor providing metallic ions in solution as a source for metal nanoparticle (NP) generation onto the GNF structures, which is commonly named a NP-decoration process [20].

The process of growing Pt/GNF using the thermal plasma system can be divided into three steps. The first step involved generating the plasma. Argon gas was fed through the sheath and central gas ports at 45 and 13 slpm respectively at a pressure of 13.79 kPa. Once a stable plasma jet with 20 kW power is achieved, the pressure inside the conical reactor was increased to 55.16 kPa and carbon precursor methane gas was delivered to the injection gas port at a flow rate of 1 slpm. Methane flow was continued for 10 minutes to grow approximately 200 mg of GNF.

The next step was to introduce a platinum precursor to the plasma. The pressure inside the reactor was lowered to 13.79 kPa and the power of the plasma torch was increased to 25 kW for this step. Platinum (IV) nitrate solution with 15 w/w% platinum [76] was chosen as the liquid precursor due to its low halide content and solubility. The salt solution was injected directly into the plasma through a viewport located 9 cm below the exit of the nozzle of the ICP torch using a stainless-steel syringe from Chemyx at a flowrate of 60 mL/hr with nitrogen as the carrier gas.

3.3 Wet chemistry and pyrolysis

Jaoun *et al* developed a method to include iron in carbon soot support using pyrolysis while investigating the importance of carbon support towards electrocatalytic activity of non-noble catalysts for oxygen reduction reaction of PEMFCs [77]. A modified version of the same method was used in this work with a platinum nitrate precursor containing 15 wt% platinum. A mass of 112.67 mg of the salt solution and 67.6 mg of pure GNF were dispersed together in 1:1 water-ethanol mixture to synthesize a 20 wt% Pt/GNF catalyst.

The mixture was sonicated in an ultrasonic bath for an hour and then heated in an oven at 100^{o}C until all the liquid evaporated. After collecting the sample from the walls of the beaker, pyrolysis was performed with argon gas at a temperature of 700^{o}C and a flow rate of 600 sccm inside a tube furnace shown in Figure 13. It is to be noted that prior comparative studies on the GNF structures made by Dr. N. Hordy using thermogravimetry analysis (TGA) indicated that degradation of the GNF structure was observed in air to start at a temperature of 775^o C. Such degradation temperature is typically in the order of 150-200^o C higher than other graphene materials tested. This is another indication of the strong crystallinity and purity of the GNF structure [78].

Figure 13: Tube furnace serving as the pyrolysis reactor used in the PPL lab.

3.4 Characterization techniques

3.4.1 Microscopy

The nanoscale nature of both the GNF and the platinum nanoparticles require high resolution imaging based on electron microscopy. Scanning electron microscope (SEM) was used to compare the surface topography of the platinum nanoparticles dispersed in the GNF and CB support. SEM detects electrons emitted from the surface of a sample after bombardment and produces a high-resolution image where secondary and backscattered electrons attribute to the resolution and contrast of the image respectively [79].

Transmission electron microscope (TEM) transmits high-energy electron beam through a thin or “electron transparent” sample (thickness below 100 nm) to gain information at atomic level [80]. TEM was used to detect the presence of platinum at nanoscale inside the GNF support.

SEM images were captured on a Hitachi SU8000 microscope and TEM images were captured on a Philips CM200 microscope.

3.4.2 Energy dispersive X-ray spectroscopy

The energy dispersive X-ray (EDX) spectroscopy is a technique used within an electron microscope to identify the elements present in specimens based on the characteristic X-rays generated by them. The specimen is bombarded with finely focused electron beam under vacuum, and the interaction between the electron beam and the specimen of interest produces X-rays with energies characteristic of atomic number of elements present in the specimen. The X-rays are detected as a function of wavelength. Heavier elements are detected more efficiently with EDX compared to lighter elements due to lower amount of X-ray emission from lighter elements. EDX should be used a qualitative analysis rather than a quantitative one [81].

EDX was used with TEM to analyze the platinum/graphene catalyst structure, indicating the composition of specific regions if interest.

3.4.3 Neutron activation analysis

Neutron activation analysis (NAA) can identify and measure traces of various elements by analyzing the gamma rays they give off after being irradiated or activated by neutrons that are in thermal equilibrium with the room temperature. The activated elements disintegrate by emitting high-energy gamma rays with extremely short half-lives in the order of ps. Analyzing these gamma rays using a technique called prompt gamma activation analysis reveal the energy of the rays and half-lives of the nuclei of the radioactive elements. This information can be used to identify the original nonradioactive elements. Nuclear reactions are independent of an atom's chemical associations enabling NAA to identify the chemical elements instead of the compounds [82].

NAA was used on the platinum/graphene nanoflake catalyst to determine the wt% of platinum in the GNF support to facilitate an appropriate comparison with a commercial catalyst with similar platinum composition. The experiment was carried out at École Polytechnique de Montréal with the SLOWPOKE reactor, an Ortec DSPEC Pro^{TM} multichannel analyzer, a Sartorius precision balance, an Ortec GEM30185-P germanium semiconductor gamma-ray detector, and the EPAA analysis software.

3.4.4 Rotating disk electrode

Several electrochemical techniques can be used to analyze the electrocatalytic performance of a fuel cell catalyst. In this thesis, rotating disk electrode (RDE) test was chosen over other techniques like cyclic voltammetry and chrono-amperometry to obtain additional insight into the oxygen reduction reaction mechanism that takes place at the cathode. In typical RDE experiments, three electrodes (working, reference and counter) are immersed in an electrolyte. The catalyst to be studied is deposited on the working electrode. A potential difference can be observed between the working electrode and the reference electrode while the current flows through the electrolyte between the counter electrode and the working electrode. Gas is bubbled through the electrolyte while a potentiostat is used to vary or record the potential difference and the current density. A simple three-electrode system is shown below in Figure 14.

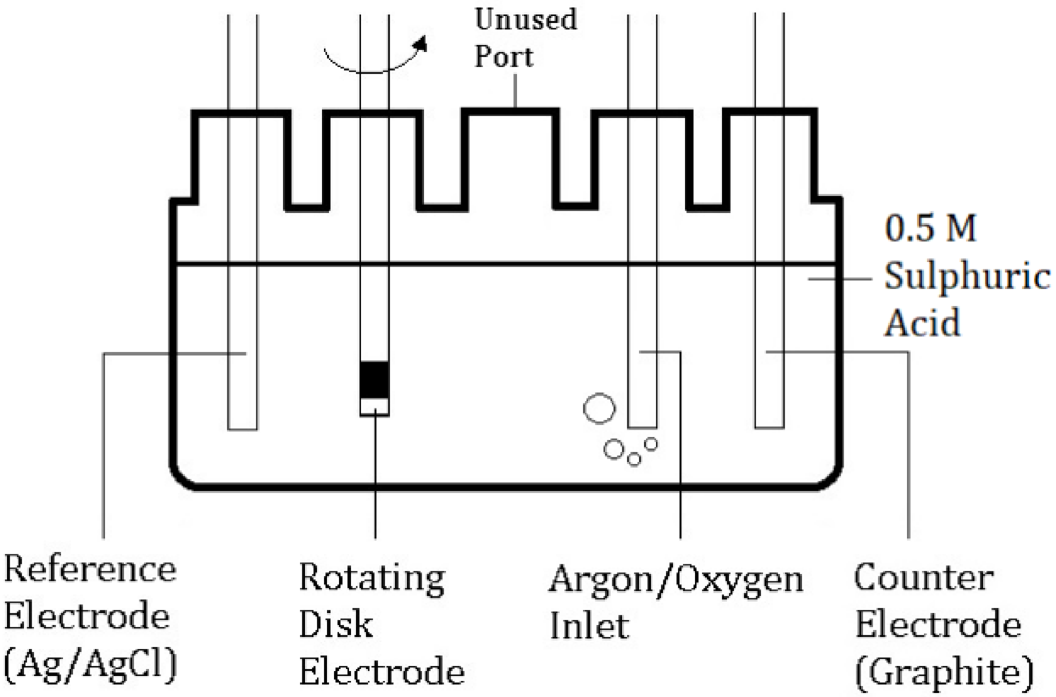

Figure 14: Schematic of custom RDE cell with three electrodes [83].

Material is delivered using forced convection to the working electrode continually in a controlled manner to measure the electrocatalytic activity of the sample catalyst. The rotating disk keeps the electrolyte solution homogeneous throughout the process. A stagnant layer that forms next to the electrode is called a Levich layer and it adheres to the electrode and rotates with it. Diffusion is the primary mode of mass transport inside the levich layer. The concentration gradient remains constant with time that results in a steady state current [84].

The catalyst ink deposited on the working electrode was prepared following the formula refined by previous researchers as shown below in Table 2.

Table 2: Catalyst ink formula

Component	**Amount**
RO Water	0.8 mL per mL of ink
Ethanol	0.2 mL per mL of ink
Nafion	4 μL per mL of ink
Nanomaterial (Pt/GNF or commercial catalyst)	1 mg per mL of ink

The ink was sonicated for an hour in an ice bath after preparation. A glassy carbon working electrode from Pine instruments was polished using a micro cloth and alumina paste for 2 minutes before each run and sonicated afterwards in RO water for 5 minutes to ensure a clean surface.

A volume of 19.6 µL of the catalyst ink was deposited onto the glassy carbon surface using a pipette. This led to a catalyst loading of 0.01 mg of per cm^2 of the glassy carbon electrode area. The working electrode was then dried overnight in a humid environment. A standard three-electrode setup was formed with an Ag/AgCl reference electrode, a platinum wire counter electrode and the glassy carbon working electrode inside a custom made RDE cell.

The RDE cell was filled with 100 mL of 0.5 M sulphuric acid. The rotational speed of the working electrode was controlled using a rotator. Each run consisted of three tests. A conditioning test was carried out while nitrogen gas was being bubbled to the electrolyte for 30 minutes. During conditioning, the voltage was swept from -1 V to 1 V at a scan rate of 100 mV/s for 50 cycles.

Next, the correction step was performed at 10 mV/s for 5 cycles to remove capacitive current contributions. The final test was obtaining ORR current after oxygen was purged into the electrolyte for 5 minutes. It was ensured that no gas bubbles were touching the working electrode. The data collection was performed using the same parameters as the correction test. Electrochemical measurements were carried out using an EZ-Stat potentiostat. The final RDE set up is shown below in Figure 15.

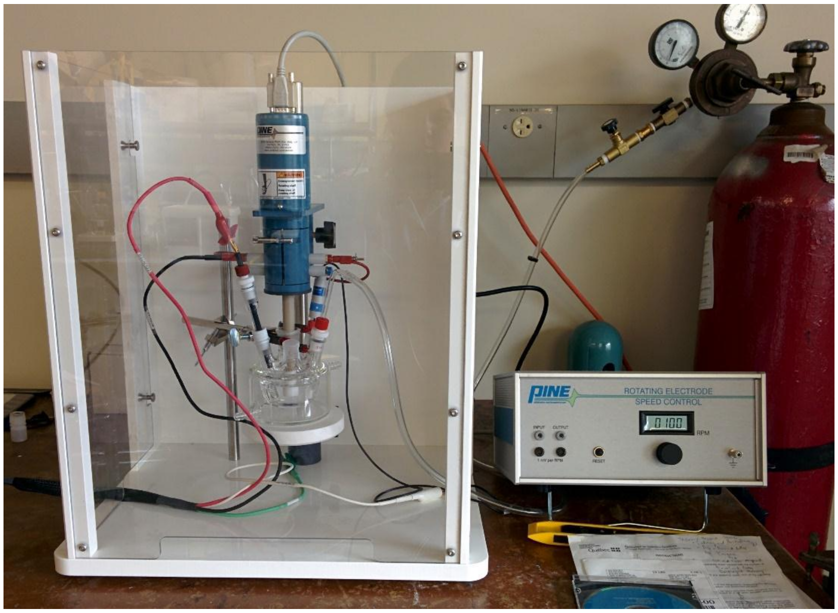

Figure 15: RDE experimental setup.

4. RESULTS AND DISCUSSION

4.1 GNF growth and introduction of platinum using thermal plasma

A Pt/GNF catalyst was synthesized in 2 steps using the thermal plasma as described in section 3.1. The TEM images and the EDX plot is presented below in Figure 16.

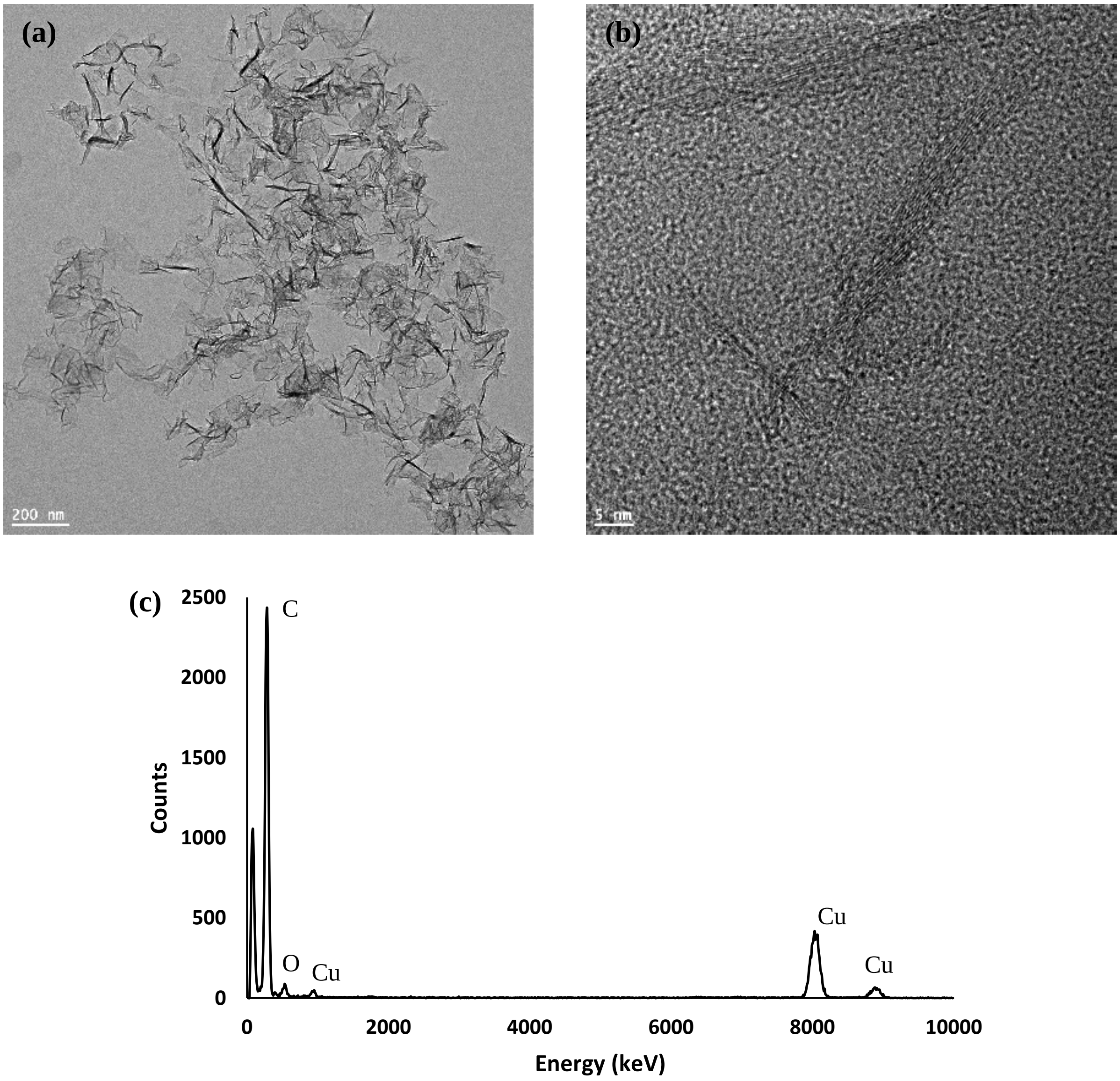

Figure 16: TEM micrographs of first sample at (a) 200 nm, (b) 5 nm scale, and (c) EDX spectra obtained from TEM.

The TEM images and the EDX plot reveal that there is no platinum present in the synthesized catalyst. The TEM images show graphitic structure of graphene nanoflakes consistent with the observation of previous researchers [74]. The source of the copper and oxygen present in the sample can be traced back to the grid supporting the sample to be analysed in TEM and the platinum nitrate salt solution respectively.

According to work published by Legrand *et al.*, weight loss up to 74% has been observed in the thermal plasma reactor during the functionalization step [18]. Taking this loss into account, a higher amount (1.93 g) of the 15% w/w platinum nitrate salt solution was introduced into the reactor to synthesize a Pt/GNF catalyst with platinum content around 20 wt%. The TEM micrographs of the new sample are presented below in Figure 17.

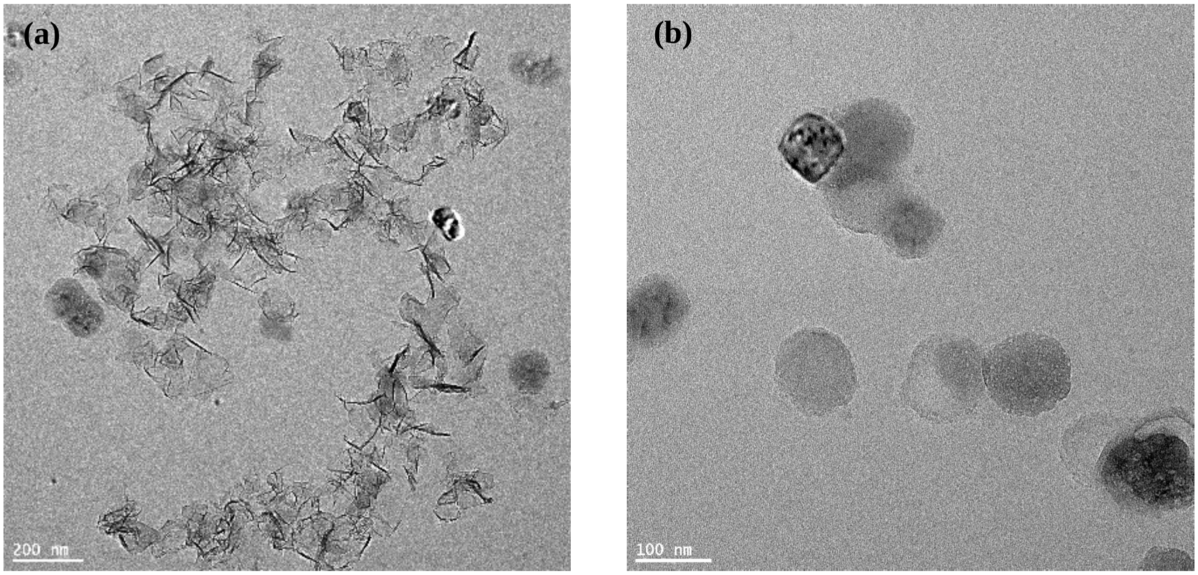

Figure 17: TEM images of the second sample at (a) 200 nm, and (b) 100 nm scale.

There was no platinum present in the catalyst sample observed through TEM, but salt crystals were observed. The presence of salt crystals can be explained by the composition of the platinum nitrate salt solution that is used as the precursor to introduce platinum to the plasma. The product specification sheet of the salt solution indicated presence of chloride content up to 0.8%

and trace amounts of sodium with a maximum of 1600 ppm [76]. Increasing the amount of the salt solution being injected resulted in a higher concentration of Na and Cl even though they are present in negligible amount in the salt solution. The EDX spectra confirmed the presence of salt with significant counts of both Na and Cl as shown below in Figure 18. The presence of copper and silica can be explained by them being present in the sample holding grid of TEM.

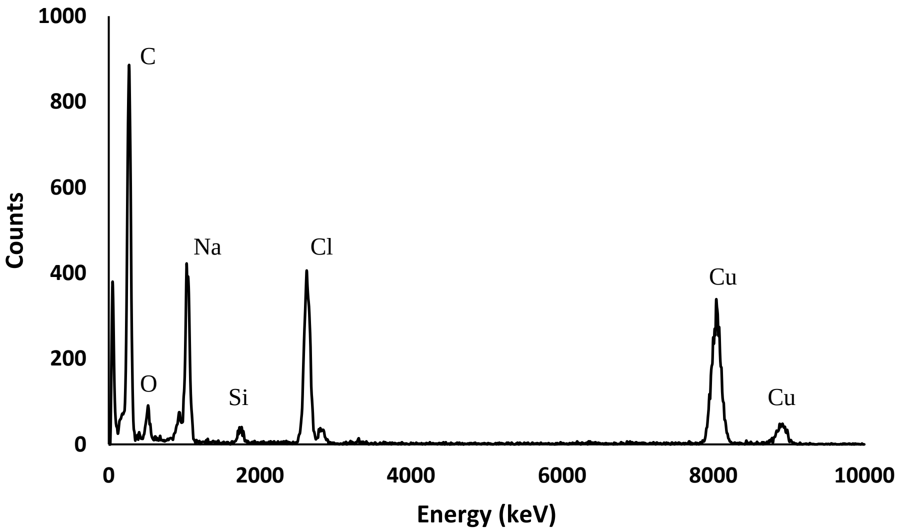

Figure 18: EDX spectra of second sample.

Visual inspection of the sample powder revealed agglomerated metal particles as shown in Figure 19.

Figure 19: Platinum agglomeration in catalyst sample marked with red circle.

SEM and EDX was used to further analyze these agglomerates. The result is shown in Figure 20. The analysis confirmed the presence of platinum in these agglomerates.

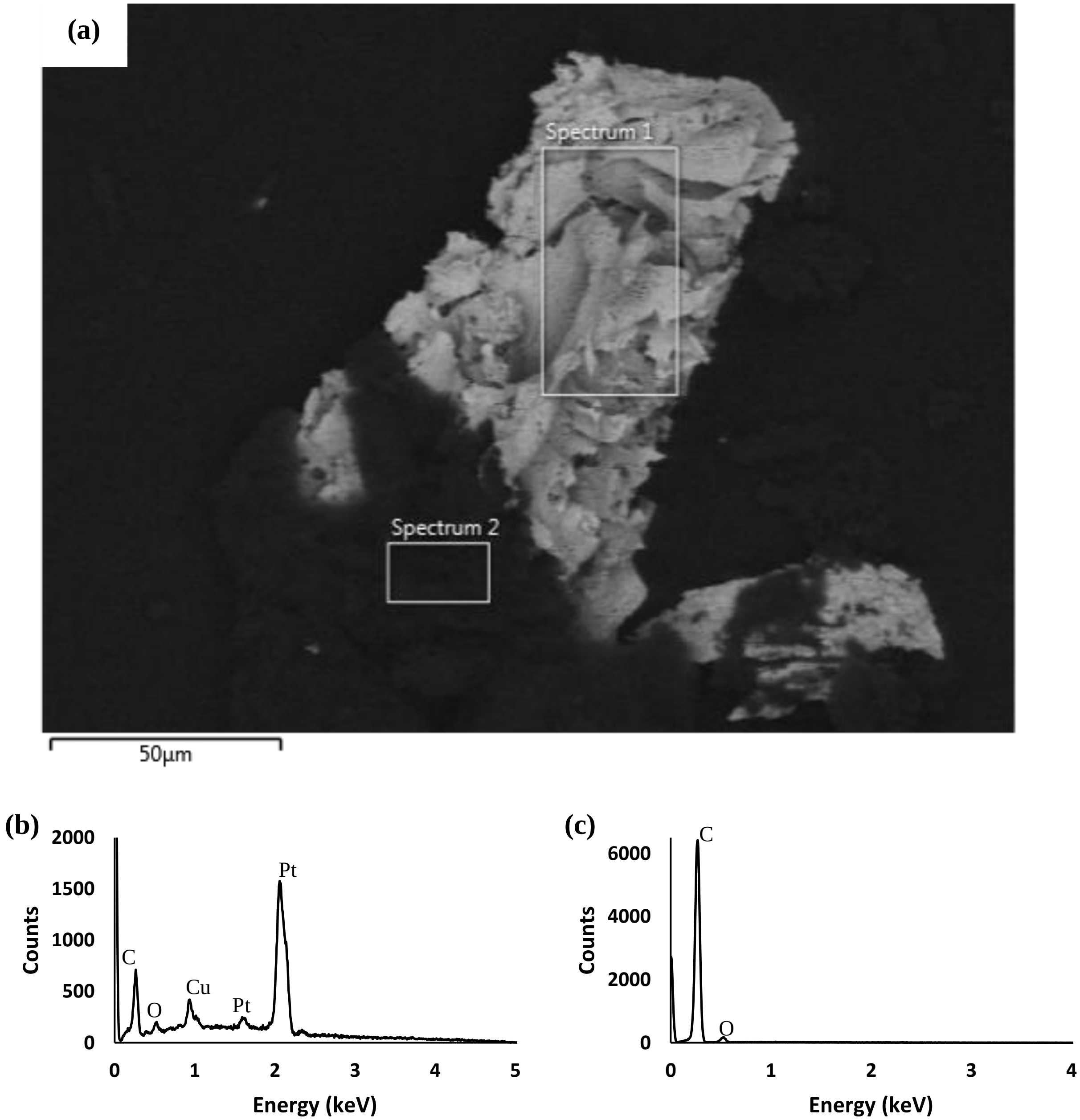

Figure 20: (a) SEM imaging of metal agglomerates with two different EDX zones marked as spectra, (b) EDX analysis of spectrum 1, and (c) EDX analysis of spectrum 2.

To understand why the functionalization step using thermal plasma failed, the temperature profile of the conical thermal plasma reactor during operation must be analyzed. The melting and boiling point of platinum is 1768^{o} C and 3825^{o} C, respectively [85]. Figure 21 shows the temperature profile inside the conical reactor during operation as modelled by Meunier *et al.* [75]. The injection point of the platinum precursor was 9 cm downstream of the plasma torch in a zone where the plasma starts to be in recombination. The liquid injection quenches the plasma even more, while the residence times of the precursor in the hotter sections is in the order of tens of milliseconds. As a result, the boiling point of platinum is not attained with such a downstream injection implying that there was no vaporization of the platinum in the system, and hence no nucleation of platinum nanoparticles.

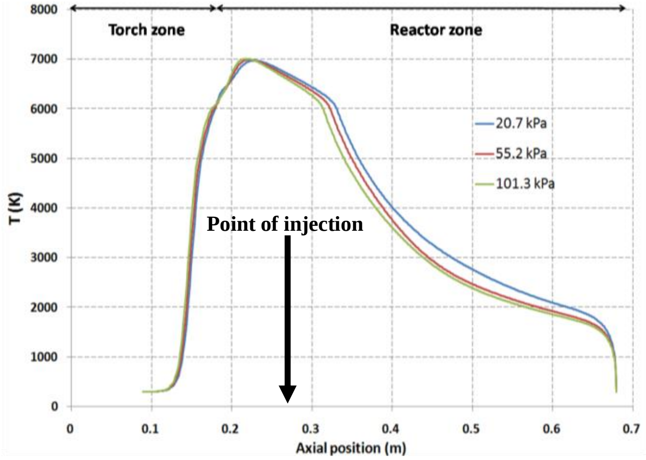

Figure 21: Temperature profile of GNF growth inside ICP thermal plasma [75].

Due to the high boiling point of platinum, the production of platinum nanoparticles requires an injection of the precursor directly into the plasma torch injection probe to enable a full vaporization of the species, followed downstream by the homogeneous nucleation of the nanoparticles in the expansion zone, and further the deposition of the nanoparticles in a decoration scheme over the GNF structure.

In the course of the present study however, probe injection was not possible. A wet chemistry technique was chosen as an alternate method to generate Pt nanoparticles on the GNF structures, as discussed below.

4.2 Introducing platinum using wet chemistry and pyrolysis

A post-processing technique using wet chemistry as discussed in Section 3.2 was used for the generation of platinum nanoparticles. The resulting sample was analyzed using TEM as shown on Figure 22.

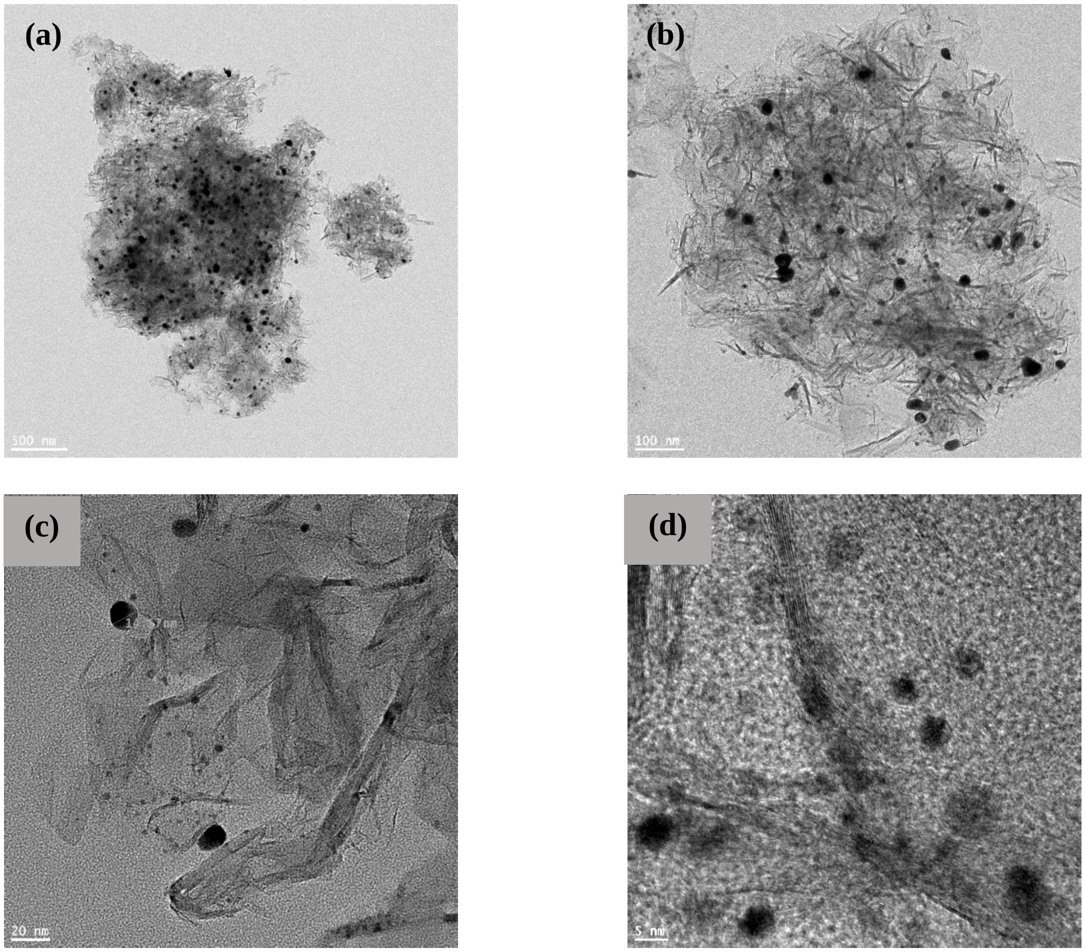

Figure 22: TEM images of Pt/GNF catalyst at (a) 500 nm, (b) 100 nm, (c) 20 nm, and (d) 5 nm scale.

The images confirmed the presence of platinum nanoparticles on the graphene nanoflakes structures. The diameter of the platinum nanoparticles is in the order of 3-4 nm (Figure 19d). While the distribution is mostly uniform, some agglomerated platinum nanoparticles can be observed with diameters as high as 14.9 nm (Figure 22b, c). The GNF structure seems to retain its graphene nature irrespective of the presence of the platinum nanoparticles. Figure 23 shows the EDX spectra obtained from these samples, confirming the presence of platinum.

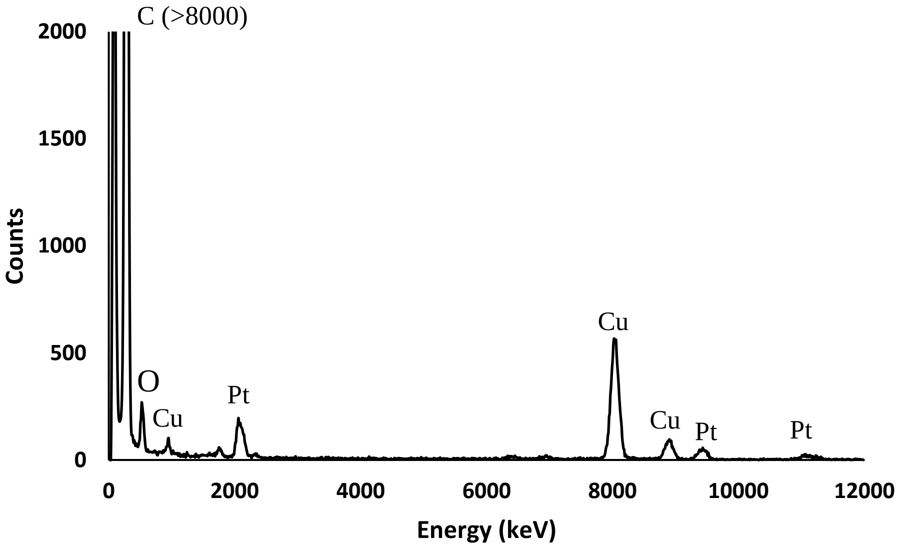

Figure 23: EDX spectra of Pt/GNF catalyst.

4.3 Rotating disk electrode tests

Preliminary tests were made using rotating disk electrode at different RPMs. The tests were carried out using an ink prepared from the Pt/GNF catalyst and loading conditions stated in Section 3.4.4. The result is presented below in Figure 24. Each curve is an average of 5 different voltammetry curves obtained at the same RPM where the standard error of the mean is less than 0.01 unit.

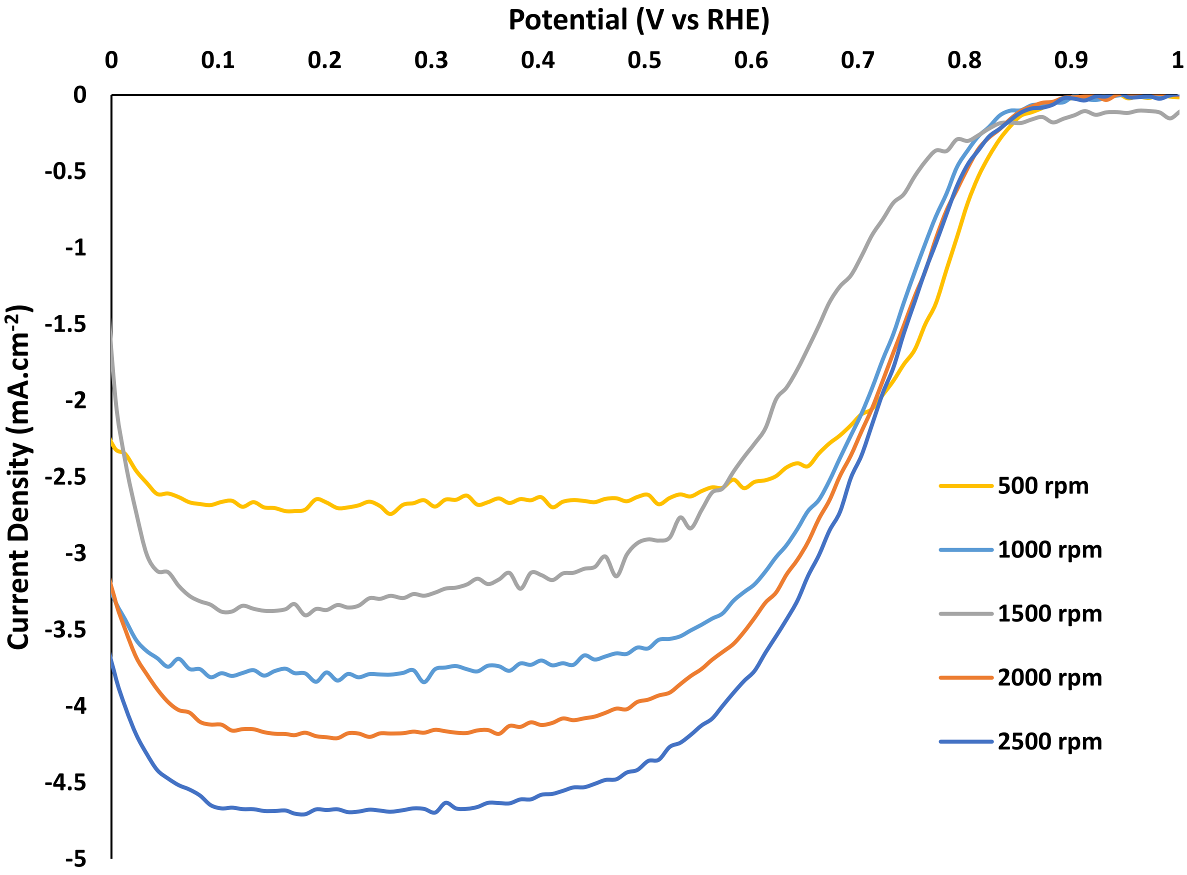

Figure 24: Current density vs potential curves at different rotational speeds obtained from first set of experiments done with Pt(20 wt%)/GNF .

While analyzing the current density vs potential curves, three parameters are given the most importance: onset potential, halfwave potential and limiting current density. Onset potential can be defined by the potential at which the reduction of oxygen starts, normally indicated by the beginning of current flow. Limiting current density is the peak current density during reduction after which the reactant depletes from the surface and the current flow drops. Halfwave potential is the potential at which half of the limiting current density is achieved.

The consistent high onset potential value (>0.8 V) at different rotational speeds confirm the presence of platinum based on literature. The limiting current density of the curves should increase with increasing rotational speed due to the decrease in mass transfer limitation [84], but the trend is inconsistent in Figure 24 as further illustrated by the values reported in Table 3.

Table 3: Values of electrocatalytic parameters of ORR in the first set of RDE test

RPM	**Current onset potential (V vs RHE)**	**Halfwave potential (V vs RHE)**	**Limiting Current Density ($mA.cm^{-2}$)**
500	0.86	0.77	-2.72
1000	0.84	0.71	-3.84
1500	0.91	0.64	-3.40
2000	0.85	0.70	-4.20
2500	0.85	0.71	-4.70

The graph obtained at 1500 rpm was inconsistent compared to the rest. It featured an unusual combination of high onset potential, low half-wave potential and a lower limiting current density compared to that of the graph obtained at 1000 rpm.

Two changes were implemented in the procedure of the RDE tests to improve the results. First, the purging time of oxygen gas was increased from five minutes to half an hour to ensure proper emulation of the fuel cell environment. Second, the RDE runs were done at a stretch without removing the electrode, i.e. the rpm was increased after one test was finished instead of carrying out the tests separately at different rotational speeds with different ink deposit as described in section 3.4.4 which increased the variability from test to test significantly. The loading condition was kept the same. The resulting plots are presented below in Figure 25.

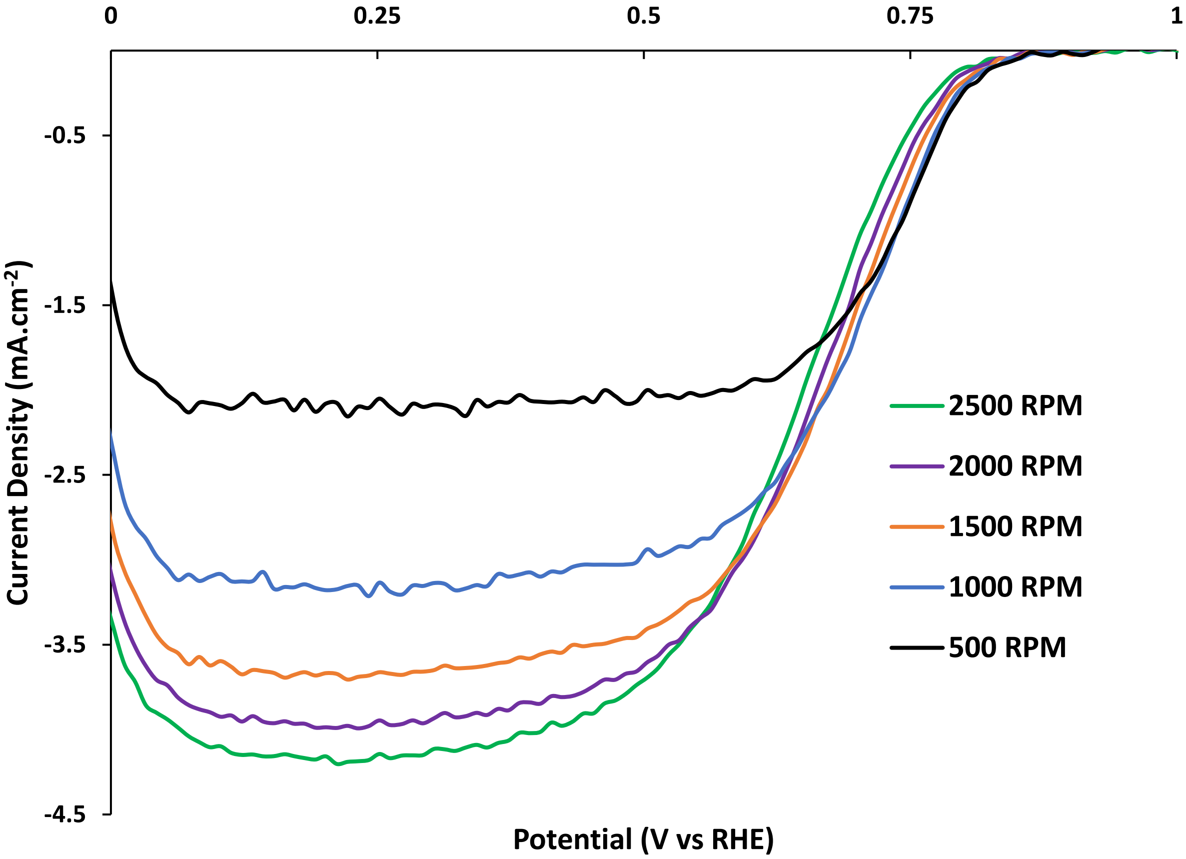

Figure 25: RDE results after increasing oxygen purging time and running tests at a stretch with same loading conditions.

The limiting current density increases with increasing rotational speed of the working electrode as expected. The onset potential of all the plots are consistent, and there is a symmetrical crossover between the curves when the mass transfer limitation kicks in limiting the peak current density. The relevant parameters are presented below in Table 4.

Table 4: Values of electrocatalytic parameters of ORR from the second set of RDE test

RPM	**Current onset potential (V vs RHE)**	**Halfwave potential (V vs RHE)**	**Limiting Current Density (mA.cm^{-2})**
500	0.82	0.73	-2.15
1000	0.82	0.70	-3.21
1500	0.82	0.67	-3.70
2000	0.81	0.66	-3.99
2500	0.81	0.64	-4.20

The electron transfer number is an important characteristic of the oxygen reduction reaction (ORR) in aqueous electrolytes as it mirrors the efficiency of oxygen conversion and provides information on the mechanism of ORR. In an acidic electrolyte, oxygen can be reduced directly to H_2O using 4 electrons or indirectly via H_2O_2 molecules using 2 electrons at the cathode of a PEMFC as shown below [86].

$$\text{Reaction pathway 1: } O_2 + 4H^+ + 4e^- \rightarrow 2H_2O$$

$$\text{Reaction pathway 2: } O_2 + 2H^+ + 2e^- \rightarrow H_2O_2$$

If the second reaction pathway is followed, H_2O_2 gets further reduced to H_2O via the following reaction.

$$H_2O_2 + 2H^+ + 2e^- \rightarrow 2H_2O$$

The two reactions happening in the second pathway can be combined to obtain the first reaction pathway. The difference between direct and indirect pathway is dictated by the release of free H_2O_2 molecules into the electrolyte [87]. A high concentration of H_2O_2 can deteriorate the proton exchange membrane of PEMFCs. This happens due to a change in membrane morphology resulting from decomposition of sulfonic acid groups in side chains. Proton conductivity and self-diffusion of water decrease significantly leading to overall reduced performance of the PEMFC [88].

The Koutecky-Levich (KL) equation written below can be used to calculate the number of electrons transferred and the heterogeneous rate constant for the ORR.

$$\frac{1}{i} = \frac{1}{i_k} + \frac{1}{0.62nFAD^{\frac{2}{3}}\omega^{\frac{1}{2}}v^{-\frac{1}{6}}C_0} \qquad \text{(Equation 1)}$$

where i_k is the heterogeneous rate constant limited current, n is the number of electrons transferred in the ORR, F is Faraday's constant (96485 $C.mol^{-1}$), C_0 is the bulk concentration of oxygen in 0.5 M H_2SO_4 ($1.1x10^{-6}$ $mol.L^{-1}$), D is the diffusion coefficient of oxygen ($1.4x10^{-5}$ $cm^2.s^{-1}$), A is the area of the electrode (0.1963 cm^2), ω is the rpm, and v is the kinematic viscosity of the 0.5M H_2SO_4 solution ($1.07x10^{-2}$ $cm^2.s^{-1}$). Plotting $\frac{1}{i}$ vs $\frac{1}{\omega^{\frac{1}{2}}}$ gives a line whose y-intercept is $\frac{1}{i_k}$. The slope of this line can be used to calculate n and the heterogeneous rate constant can be calculated using Equation 2.

$$i_k = nFAk^oC_0 \qquad \text{(Equation 2)}$$

where k^o is the heterogeneous rate constant (in cm/s) and the other parameters are as above.

The KL equations facilitated the calculation of the number of electrons transferred by plotting the inverse of limiting current vs the inverse of square root of rotational speed of the working electrode. The result is presented below in Figure 26.

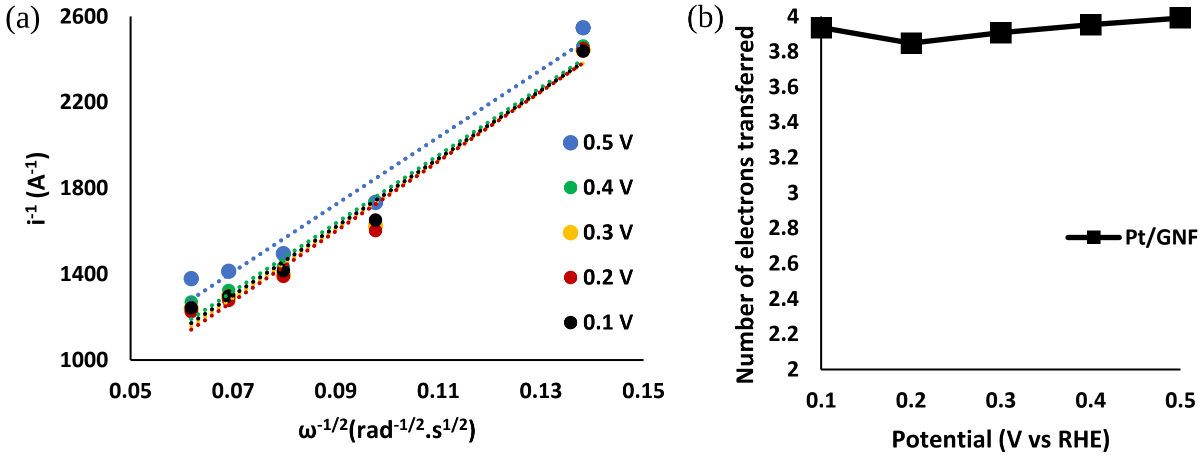

Figure 26: (a) Inverse of current (i^{-1}) vs inverse of the root of rotational speed ($w^{-1/2}$), and (b) the number of elctrons transferred at different potentials of interest.

The lines overlap with each other illustrating consistency in the electron transfer process from 0.1 to 0.5 V where peak current densities occur indicating the reduction reaction. This is further confirmed by the number of electrons transferred calculated from the slope of these lines as shown in Figure 26b. A consistent number of 4 electrons were transferred in the potential range of 0.1 – 0.5 V. This means oxygen was directly converted to OH^- rather than going through the step of H_2O_2 production. The change in slope of the lines in Figure 26a with varying rotational speed is very negligible and only noticeable in the plot because of the magnification of the axes.

The heterogeneous reaction rate constants at different potentials are presented below in Table 5.

Table 5: Heterogenoeous reaction rate constant during ORR

Potential (V vs RHE)	**Reaction rate constant** ($cm.s^{-1}$)
0.1	$6.4x10^{-2}$
0.2	$9.1x10^{-2}$
0.3	$7.2x10^{-2}$
0.4	$5.7x10^{-2}$
0.5	$3.8x10^{-2}$

The peak current density values are achieved between 0.2 and 0.3 V as observed in Figure 25. The reaction rate constant peaks in the same range which is understandable as the reaction rate constant should be highest when the limiting current density is at its highest value.

4.4 Neutron activation analysis

EDX spectra of the Pt/GNF catalyst confirmed the presence of platinum in the sample catalyst but it gave only a qualitative picture. It is important to confirm the wt% of platinum in the Pt/GNF catalyst before comparing its performance to that of an industrial catalyst with a similar platinum composition. To get the quantitative amount of platinum present in the sample, neutron activation analysis (NAA) was carried out.

A mass of 36.8 mg of the synthesized platinum/graphene nanoflakes catalyst was used to perform NAA. Pt concentration was found to be 22.9% with an uncertainty of 0.9% which is close to the target concentration of 20% during synthesis.

4.5 Comparison with industrial Pt-based catalyst using carbon black particles

A concentration of 20% Platinum on Vulcan XC-72R sold by FuelCellStore [89] was used as the industrial standard to compare the electrocatalytic performance of the Pt/GNF catalyst synthesized in the present work. This concentration was specifically chosen to match approximately the Pt concentration achieved in the present Pt/GNF samples

4.5.1 Structure (SEM)

SEM images presented below in Figure 27 show the typical aggregated monodispersed spherical morphology of carbon black [90] and flake-like morphology consistent with graphene nanoflakes [17]. Platinum nanoparticles can be seen uniformly dispersed on the surface of both samples with similar particle size ranging from 3-4 nm. With similar platinum loading and particle size, the only difference between the samples lies in the carbon support. The agglomerated spherical carbon black offers less catalytic sites compared to the folding sheets of GNF with more surface area.

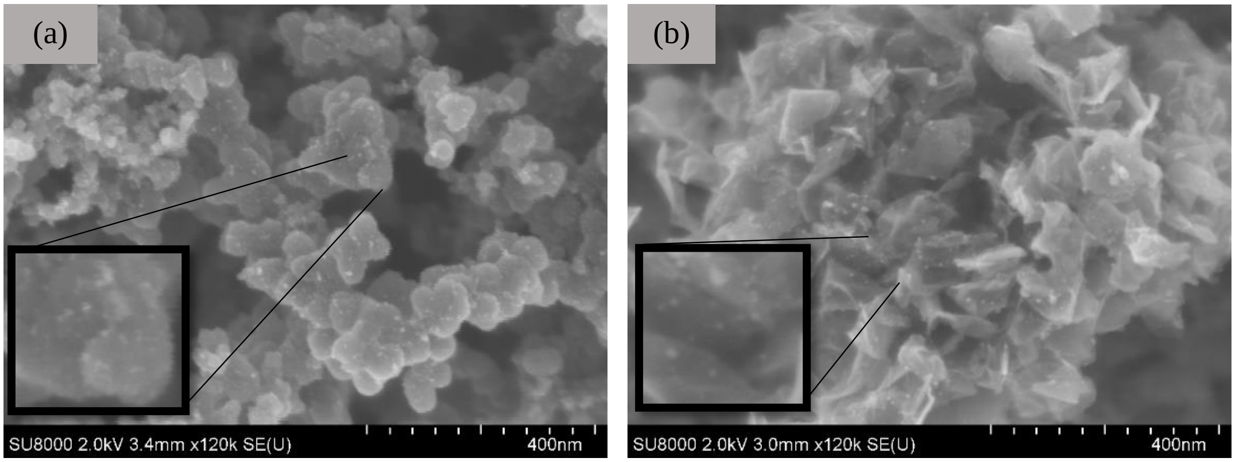

Figure 27: SEM micrographs of (a) Pt/VulcanXC72R and (b) Pt/GNF at 400 nm.

4.5.2 RDE tests

The current density vs RHE plots at different rpms for inks prepared from the commercial and in-house catalysts are presented below in Figure 28.

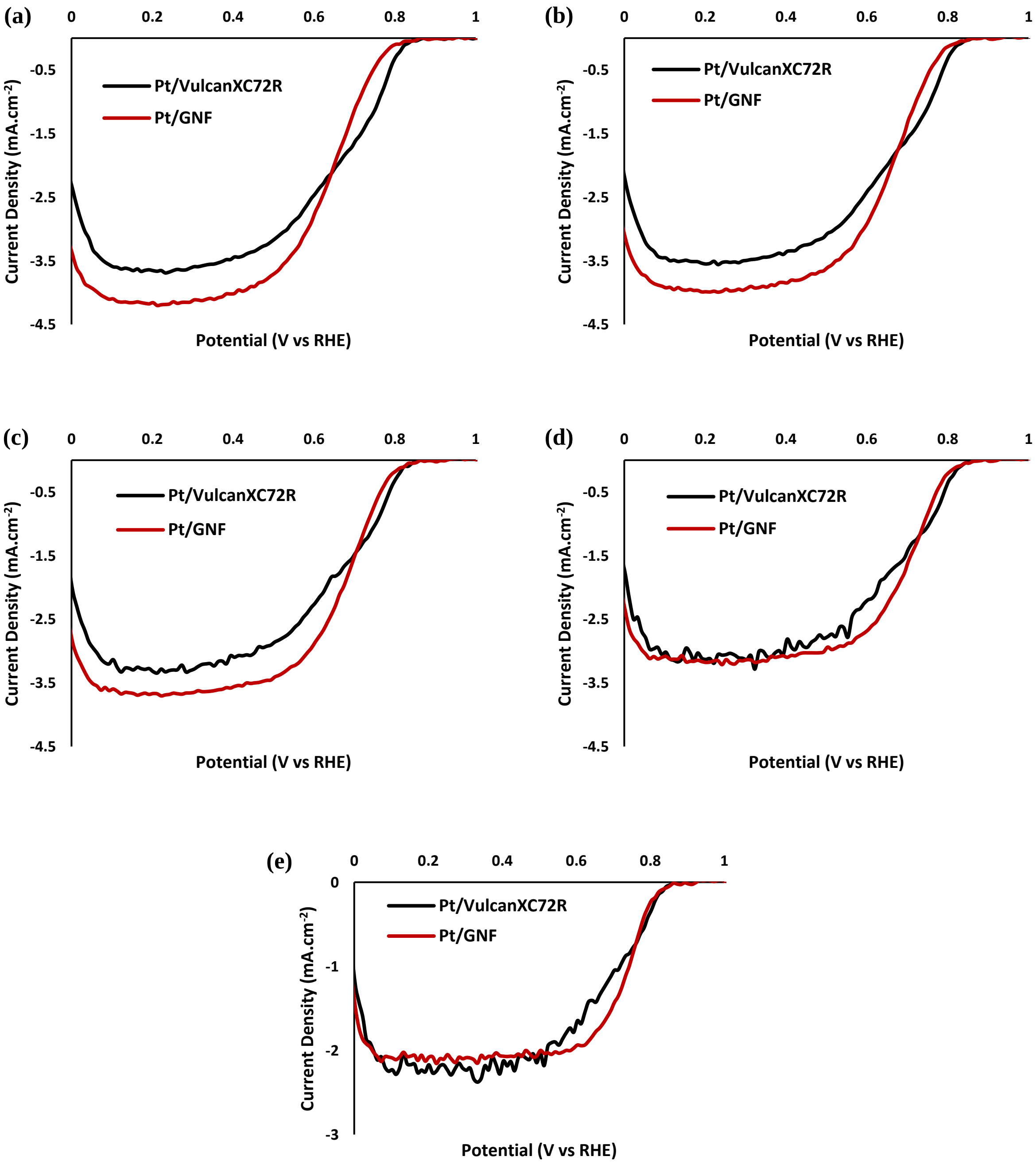

Figure 28: Current density vs RHE at (a) 2500 rpm, (b) 2000 rpm, (c) 1500 rpm, (d) 1000 rpm and (e) 500 rpm.

At high rotational speed the Pt/GNF ink outperforms the Pt/VulcanXC72 ink. The performance of the inks is similar at lower rpms (<1000 rpm). The onset potential value of the two inks is similar confirming the presence of platinum in them. The Pt/VulcanXC72R plots demonstrate one extra point of inflection at approximately 0.7 V which forces the two plots to cross each other and results in a consistent half-wave potential even at different rpms. The initial increase in the current density is higher for the commercial catalyst at higher potentials but as the potential decreases the performance deteriorates and the Pt/GNF catalyst reaches a higher limiting current density faster which is desirable. This results from a change in reaction mechanism at 0.7 V for the commercial catalyst ink. The key electrochemical values from the RDE tests are presented below in Table 6.

Table 6: Electrocatalytic parameters obtained from RDE tests

RPM	**Catalyst**	**Current onset potential (V vs RHE)**	**Halfwave potential (V vs RHE)**	**Limiting current density (mA.cm^{-2})**
500	Pt/GNF	0.82	0.73	-2.15
	Pt/VulcanXC72R	0.83	0.68	-2.38
1000	Pt/GNF	0.82	0.70	-3.21
	Pt/VulcanXC72R	0.82	0.67	-3.28
1500	Pt/GNF	0.82	0.67	-3.70
	Pt/VulcanXC72R	0.82	0.67	-3.33
2000	Pt/GNF	0.81	0.66	-3.99
	Pt/VulcanXC72R	0.82	0.67	-3.56
2500	Pt/GNF	0.81	0.64	-4.20
	Pt/VulcanXC72R	0.82	0.67	-3.69

High rotational speeds eradicate mass transfer limitation to the surface of the working electrode. The difference in electrocatalytic activity observed at higher rotational speeds can be attributed to the structural difference of the carbon support of the two catalysts. As the voltage decreases and the reduction reaction intensifies the catalyst sites offered by the Pt/VulcanXC72R becomes less accessible to oxygen molecules leading to a reduced current density compared to the Pt/GNF catalyst. The consistent extra point of inflection, which is responsible for lowering the limiting current density, observed in the curves of the commercial catalyst supports this hypothesis.

4.5.3 Catalyst ink aging

The catalyst ink prepared from two sample catalysts were stored in glass vials and RDE tests were run once a month in similar conditions. The limiting current density decreases over time for catalyst inks made with both Pt/GNF and Pt/VulcanXC72R as shown below in Figure 29. This trend can be explained by agglomeration of nanoparticles or oxidation occurring due to the presence of air on top of the ink inside the vial. The inks were sonicated for 5 minutes before running each test making performance degradation due to agglomeration less likely.

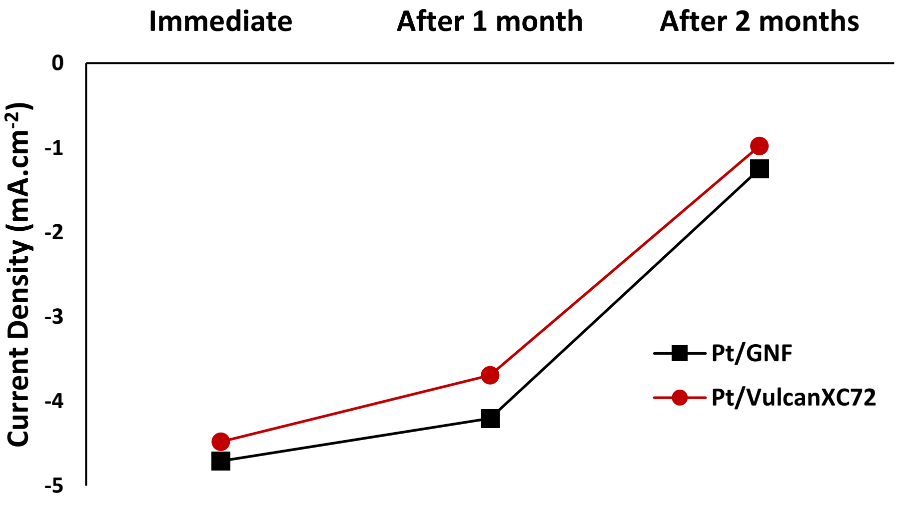

Figure 29: Limiting current density for a rotational speed of 2500 rpm.

5. CONCLUSION

5.1 Summary

This master's thesis aimed to synthesize and investigate the performance of a platinum-based catalyst with graphene nanoflakes as the support for proton exchange membrane fuel cells compared to its commercial counterparts that have carbon black as the carbon support. The original plan was to synthesize the catalyst using thermal plasma, but limitations arising from high boiling point of platinum restricted the platinum to be introduced at a nanoscale level onto the graphene nanoflakes support. A wet chemistry technique followed by pyrolysis was used to successfully synthesize the catalyst.

The presence of platinum nanoparticles did not interfere with the inherent high surface area and graphitic structure of the graphene nanoflakes support. Electrocatalytic activity of the catalyst towards oxygen reduction reaction in acidic medium using rotating disk electrode tests revealed that four electrons were transferred, and the reaction mechanism involved direct conversion of oxygen gas to OH^-. The platinum/graphene nanoflakes catalyst demonstrated superior performance when mass transfer limitation was removed at high rotational speeds compared to a commercial carbon black supported catalyst. This superior performance, with a similar platinum dispersal in the two catalysts, can be attributed to the availability of more catalytic sites in the graphene nanoflakes structure.

5.2 Recommendations for future work

Based on the findings of this thesis, the author recommends the following for future work.

1) To further explore the thermal plasma technique in introducing platinum onto the GNF support, the precursor should be injected using the ICP torch injection probe which will lead to the precursor's vaporization and dispersal at nanoscale.
2) Introduction of defects in the pure graphene nanoflakes support with platinum nanoparticles should be explored. A low amount of defect could lead to higher catalytic activity without compromising the high surface area of the support.
3) The stability of catalysts is mainly related to the degradation of the catalyst support by corrosion. While the GNF structure already showed higher stability of operation in PEMFC environment, long stability tests in PEMFC environments should be made to effectively compare the behavior of carbon black and GNF in real operating conditions.

REFERENCES

[1] “Fuel Cell Systems Explained - Fuel Cell Systems Explained - Wiley Online Library.” [Online]. Available: https://onlinelibrary.wiley.com/doi/pdf/10.1002/9781118706992. [Accessed: 31-Jan-2019].

[2] T. Koppel, *Powering the Future :: The Ballard Fuel Cell and the Race to Change the World*. John Wiley & Sons Canada, Limited, 1999.

[3] F. E. Office and F. Ltd, “Development of Prototype Micro Fuel Cells for Mobile Electronics,” *FUJITSU Sci Tech J*, p. 10, 2005.

[4] H.-P. Chang, C.-L. Chou, Y.-S. Chen, T.-I. Hou, and B.-J. Weng, “The design and cost analysis of a portable PEMFC UPS system,” *Int. J. Hydrog. Energy*, vol. 32, no. 3, pp. 316–322, Mar. 2007.

[5] L. Barelli, G. Bidini, and A. Ottaviano, “Optimization of a PEMFC/battery pack power system for a bus application,” *Appl. Energy*, vol. 97, pp. 777–784, Sep. 2012.

[6] “Dynamic analysis of PEMFC-based CHP systems for domestic application - ScienceDirect.” [Online]. Available: https://www.sciencedirect.com/science/article/pii/S0306261911005794. [Accessed: 31-Jan-2019].

[7] S. Erbach *et al.*, “Influence of operating conditions on permeation of CO2 through the membrane in an automotive PEMFC system,” *Int. J. Hydrog. Energy*, Nov. 2018.

[8] “Map | Hydrogen Filling Stations | netinform.” [Online]. Available: https://www.netinform.net/h2/H2Stations/H2Stations.aspx. [Accessed: 01-Feb-2019].

[9] “US DRIVE Fuel Cell Technical Team Roadmap,” *Energy.gov*. [Online]. Available: https://www.energy.gov/eere/vehicles/downloads/us-drive-fuel-cell-technical-team-roadmap. [Accessed: 01-Feb-2019].

[10] A. Wilson, G. Kleen, and D. Papageorgopoulos, “Fuel Cell System Cost - 2017,” p. 12, Sep. 2017.

[11] “DOE Technical Targets for Polymer Electrolyte Membrane Fuel Cell Components,” *Energy.gov*. [Online]. Available: https://www.energy.gov/eere/fuelcells/doe-technical-targets-polymer-electrolyte-membrane-fuel-cell-components. [Accessed: 01-Feb-2019].

[12] F. Jaouen, F. Charreteur, and J. P. Dodelet, “Fe-Based Catalysts for Oxygen Reduction in PEMFCs Importance of the Disordered Phase of the Carbon Support,” *J. Electrochem. Soc.*, vol. 153, no. 4, pp. A689–A698, Apr. 2006.

[13] G. S. Tasic, S. S. Miljanic, M. P. Marceta Kaninski, D. P. Saponjic, and V. M. Nikolic, “Non-noble metal catalyst for a future Pt free PEMFC,” *Electrochem. Commun.*, vol. 11, no. 11, pp. 2097–2100, Nov. 2009.

[14] H. Zhong, H. Zhang, G. Liu, Y. Liang, J. Hu, and B. Yi, “A novel non-noble electrocatalyst for PEM fuel cell based on molybdenum nitride,” *Electrochem. Commun.*, vol. 8, no. 5, pp. 707–712, May 2006.

[15] K. Jayasayee, J. A. R. V. Veen, T. G. Manivasagam, S. Celebi, E. J. M. Hensen, and F. A. de Bruijn, “Oxygen reduction reaction (ORR) activity and durability of carbon supported PtM (Co, Ni, Cu) alloys: Influence of particle size and non-noble metals,” *Appl. Catal. B Environ.*, vol. 111–112, pp. 515–526, Jan. 2012.

[16] P.-A. Pascone, D. Berk, and J.-L. Meunier, “A stable and active iron catalyst supported on graphene nano-flakes for the oxygen reduction reaction in polymer electrolyte membrane fuel cells,” *Catal. Today*, vol. 211, pp. 162–167, Aug. 2013.

[17] R. Pristavita, J.-L. Meunier, and D. Berk, “Carbon Nano-Flakes Produced by an Inductively Coupled Thermal Plasma System for Catalyst Applications,” *Plasma Chem. Plasma Process.*, vol. 31, no. 2, pp. 393–403, Apr. 2011.

[18] U. Legrand, N.-Y. Mendoza Gonzalez, P. Pascone, J.-L. Meunier, and D. Berk, “Synthesis and in-situ oxygen functionalization of deposited graphene nanoflakes for nanofluid generation,” *Carbon*, vol. 102, no. Supplement C, pp. 216–223, Jun. 2016.

[19] “Nitrogen doping of graphene nanoflakes by thermal plasma as catalyst for oxygen reduction in Proton Exchange Membrane fuel cells - IEEE Conference Publication.” [Online]. Available: https://ieeexplore.ieee.org/abstract/document/6322208. [Accessed: 01-Feb-2019].

[20] U. Legrand, J.-L. Meunier, and D. Berk, “Addition of Sulphur to Graphene Nanoflakes Using Thermal Plasma for Oxygen Reduction Reaction in Alkaline Medium,” *Plasma Chem. Plasma Process.*, vol. 37, no. 3, pp. 841–856, 2017.

[21] U. Legrand, J.-L. Meunier, and D. Berk, “Iron functionalization on graphene nanoflakes using thermal plasma for catalyst applications,” *Appl. Catal. Gen.*, vol. 528, pp. 36–43, 2016.

[22] V. S. Bagotsky, *Fuel Cells: Problems and Solutions*. John Wiley & Sons, 2012.

[23] “Wärtsilä Introduces Gas-Fueled Version of ‘World’s Most Efficient 4-Stroke Diesel Engine,’” *gCaptain*, 20-Nov-2017. [Online]. Available: https://gcaptain.com/wartsila-introduces-gas-fueled-version-of-worlds-most-efficient-4-stroke-diesel-engine/. [Accessed: 15-Feb-2019].

[24] G. T. Services, U. Contract, and N. De-am-ft, *Fuel Cell Handbook (Seventh Edition) By*. .

[25] J. M. Andújar and F. Segura, “Fuel cells: History and updating. A walk along two centuries,” *Renew. Sustain. Energy Rev.*, vol. 13, no. 9, pp. 2309–2322, Dec. 2009.

[26] “Proton-exchange membrane fuel cell,” *Wikipedia*. 14-Feb-2019.

[27] "On The Shoulders of Titans - Ch7-4." [Online]. Available: https://history.nasa.gov/SP-4203/ch7-4.htm. [Accessed: 02-Feb-2019].

[28] K. A. Mauritz and R. B. Moore, "State of Understanding of Nafion," *Chem. Rev.*, vol. 104, no. 10, pp. 4535–4586, Oct. 2004.

[29] "Nafion," *Wikipedia*. 25-Jan-2019.

[30] V. Mehta and J. S. Cooper, "Review and analysis of PEM fuel cell design and manufacturing," *J. Power Sources*, vol. 114, no. 1, pp. 32–53, Feb. 2003.

[31] "Carbon Materials for Fuel Cells | SpringerLink." [Online]. Available: https://link.springer.com/chapter/10.1007/978-94-007-7708-8_7. [Accessed: 02-Feb-2019].

[32] S. D. Thompson, L. R. Jordan, and M. Forsyth, "Platinum electrodeposition for polymer electrolyte membrane fuel cells," *Electrochimica Acta*, vol. 46, no. 10, pp. 1657–1663, Mar. 2001.

[33] "A New Approach to the Problem of Carbon Monoxide Poisoning in Fuel Cells Operating at Low Temperatures." [Online]. Available: http://jes.ecsdl.org/content/135/10/2651.abstract. [Accessed: 02-Feb-2019].

[34] L. P. L. Carrette, K. A. Friedrich, M. Huber, and U. Stimming, "Improvement of CO tolerance of proton exchange membrane (PEM) fuel cells by a pulsing technique," *Phys. Chem. Chem. Phys.*, vol. 3, no. 3, pp. 320–324, 2001.

[35] "Electrocatalysis by ad-atoms: Part III. Enhancement of the oxidation of carbon monoxide on platinum by ruthenium ad-atoms - ScienceDirect." [Online]. Available: https://www.sciencedirect.com/science/article/pii/S0022072875802622. [Accessed: 02-Feb-2019].

[36] X. Yu and S. Ye, “Recent advances in activity and durability enhancement of Pt/C catalytic cathode in PEMFC. Part I. Physico-chemical and electronic interaction between Pt and carbon support, and activity enhancement of Pt/C catalyst,” *J. Power Sources*, vol. 172, no. 1, pp. 133–144, 2007.

[37] A. Wieckowski, E. R. Savinova, and C. G. Vayenas, *Catalysis and Electrocatalysis at Nanoparticle Surfaces*. CRC Press, 2003.

[38] E. Hegenberger, N. L. Wu, and J. Phillips, “Evidence of strong interaction between iron particles and an activated carbon support,” *J. Phys. Chem.*, vol. 91, no. 19, pp. 5067–5071, 1987.

[39] C. Bittencourt *et al.*, “Platinum-carbon nanotube interaction,” *Chem. Phys. Lett.*, vol. 462, no. 4–6, pp. 260–264, 2008.

[40] E. Antolini and E. R. Gonzalez, “Ceramic materials as supports for low-temperature fuel cell catalysts,” *Solid State Ion.*, vol. 180, no. 9–10, pp. 746–763, 2009.

[41] “The role of carbon in fuel cells - ScienceDirect.” [Online]. Available: https://www.sciencedirect.com/science/article/pii/S0378775306003466. [Accessed: 03-Feb-2019].

[42] R. Zacharia, S. -u. Rather, S. W. Hwang, and K. S. Nahm, “Spillover of physisorbed hydrogen from sputter-deposited arrays of platinum nanoparticles to multi-walled carbon nanotubes,” *Chem. Phys. Lett.*, vol. 434, no. 4–6, pp. 286–291, 2007.

[43] Y. Shao, G. Yin, J. Wang, Y. Gao, and P. Shi, “Multi-walled carbon nanotubes based Pt electrodes prepared with in situ ion exchange method for oxygen reduction,” *J. Power Sources*, vol. 161, no. 1, pp. 47–53, 2006.

[44] T. M. Day, P. R. Unwin, and J. V. Macpherson, “Factors controlling the electrodeposition of metal nanoparticles on pristine single walled carbon nanotubes,” *Nano Lett.*, vol. 7, no. 1, pp. 51–57, 2007.

[45] S. Park *et al.*, “Polarization losses under accelerated stress test using multiwalled carbon nanotube supported Pt catalyst in PEM fuel cells,” *J. Electrochem. Soc.*, vol. 158, no. 3, pp. B297–B302, 2011.

[46] “Carbon nanotubes: directions and perspectives in oral regenerative medicine. - PubMed - NCBI.” [Online]. Available: https://www.ncbi.nlm.nih.gov/pubmed/23677650. [Accessed: 03-Feb-2019].

[47] S. Sharma and B. G. Pollet, “Support materials for PEMFC and DMFC electrocatalysts—A review,” *J. Power Sources*, vol. 208, pp. 96–119, Jun. 2012.

[48] J.-S. Zheng, X.-S. Zhang, P. Li, J. Zhu, X.-G. Zhou, and W.-K. Yuan, “Effect of carbon nanofiber microstructure on oxygen reduction activity of supported palladium electrocatalyst,” *Electrochem. Commun.*, vol. 9, no. 5, pp. 895–900, 2007.

[49] M. J. Palmeri, K. W. Putz, T. Ramanathan, and L. C. Brinson, “Multi-scale reinforcement of CFRPs using carbon nanofibers,” *Compos. Sci. Technol.*, vol. 71, no. 2, pp. 79–86, Jan. 2011.

[50] S. Kang *et al.*, “Stability and durability of PtRu catalysts supported on carbon nanofibers for direct methanol fuel cells,” *Int. J. Hydrog. Energy*, vol. 37, no. 5, pp. 4685–4693, Mar. 2012.

[51] R. Ryoo, S. H. Joo, and S. Jun, “Synthesis of highly ordered carbon molecular sieves via template-mediated structural transformation,” *J. Phys. Chem. B*, vol. 103, no. 37, pp. 7743–7746, 1999.

[52] J. Ding, K.-Y. Chan, J. Ren, and F.-S. Xiao, “Platinum and platinum-ruthenium nanoparticles supported on ordered mesoporous carbon and their electrocatalytic performance for fuel cell reactions,” *Electrochimica Acta*, vol. 50, no. 15, pp. 3131–3141, 2005.

[53] R. Liu, D. Wu, X. Feng, and K. Müllen, “Nitrogen-doped ordered mesoporous graphitic arrays with high electrocatalytic activity for oxygen reduction,” *Angew. Chem. - Int. Ed.*, vol. 49, no. 14, pp. 2565–2569, 2010.

[54] A. Eftekhari and Z. Fan, “Ordered mesoporous carbon and its applications for electrochemical energy storage and conversion,” *Mater. Chem. Front.*, vol. 1, no. 6, pp. 1001–1027, 2017.

[55] G. M. Swain, “The use of CVD diamond thin films in electrochemical systems,” *Adv. Mater.*, vol. 6, no. 5, pp. 388–392, 1994.

[56] F. Montilla, E. Morallón, I. Duo, C. Comninellis, and J. L. Vázquez, “Platinum particles deposited on synthetic boron-doped diamond surfaces. Application to methanol oxidation,” *Electrochimica Acta*, vol. 48, no. 25–26, pp. 3891–3897, 2003.

[57] T. A. Ivandini, R. Sato, Y. Makide, A. Fujishima, and Y. Einaga, “Pt-implanted boron-doped diamond electrodes and the application for electrochemical detection of hydrogen peroxide,” *Diam. Relat. Mater.*, vol. 14, no. 11–12, pp. 2133–2138, 2005.

[58] J. A. Bennett, Y. Show, S. Wang, and G. M. Swain, “Pulsed galvanostatic deposition of Pt particles on microcrystalline and nanocrystalline diamond thin-film electrodes I. Characterization of as-deposited metal/diamond surfaces,” *J. Electrochem. Soc.*, vol. 152, no. 5, pp. E184–E192, 2005.

[59] X. Lu, J. Hu, J. S. Foord, and Q. Wang, “Electrochemical deposition of Pt-Ru on diamond electrodes for the electrooxidation of methanol,” *J. Electroanal. Chem.*, vol. 654, no. 1–2, pp. 38–43, 2011.

[60] “Boron doped diamond thin films on large area Ti6Al4V substrates for electrochemical application.” [Online]. Available: http://www.scielo.br/scielo.php?script=sci_arttext&pid=S1516-14392003000100011. [Accessed: 03-Feb-2019].

[61] K. S. Novoselov *et al.*, “Two-dimensional gas of massless Dirac fermions in graphene,” *Nature*, vol. 438, no. 7065, pp. 197–200, 2005.

[62] E. Antolini, “Graphene as a new carbon support for low-temperature fuel cell catalysts,” *Appl. Catal. B Environ.*, vol. 123–124, pp. 52–68, Jul. 2012.

[63] Y.-C. Cao, C. Xu, X. Wu, X. Wang, L. Xing, and K. Scott, “A poly (ethylene oxide)/graphene oxide electrolyte membrane for low temperature polymer fuel cells,” *J. Power Sources*, vol. 196, no. 20, pp. 8377–8382, Oct. 2011.

[64] S. Böhm, “Graphene against corrosion,” *Nat. Nanotechnol.*, vol. 9, pp. 741–742, Oct. 2014.

[65] F. Chu *et al.*, “Nitrogen-doped three-dimensional graphene-supported platinum catalysts for polymer electrolyte membrane fuel cells application,” *Funct. Mater. Lett.*, vol. 11, no. 01, p. 1850015, Jan. 2018.

[66] “A roadmap for graphene | Nature.” [Online]. Available: https://www.nature.com/articles/nature11458. [Accessed: 03-Feb-2019].

[67] D.-S. Kim, E. F. A. Zeid, and Y.-T. Kim, “Additive treatment effect of TiO2 as supports for Pt-based electrocatalysts on oxygen reduction reaction activity,” *Electrochimica Acta*, vol. 55, no. 11, pp. 3628–3633, 2010.

[68] X. Zhu, H. Zhang, Y. Zhang, Y. Liang, X. Wang, and B. Yi, “An ultrathin self-humidifying membrane for PEM fuel cell application: Fabrication, characterization, and experimental analysis,” *J. Phys. Chem. B*, vol. 110, no. 29, pp. 14240–14248, 2006.

[69] H. Chhina, S. Campbell, and O. Kesler, “Ex situ evaluation of tungsten oxide as a catalyst support for PEMFCs,” *J. Electrochem. Soc.*, vol. 154, no. 6, pp. B533–B539, 2007.

[70] G. D. Yadav and J. J. Nair, “Sulfated zirconia and its modified versions as promising catalysts for industrial processes,” *Microporous Mesoporous Mater.*, vol. 33, no. 1–3, pp. 1–48, 1999.

[71] A. Lewera, L. Timperman, A. Roguska, and N. Alonso-Vante, “Metal–Support Interactions between Nanosized Pt and Metal Oxides (WO3 and TiO2) Studied Using X-ray Photoelectron Spectroscopy,” *J. Phys. Chem. C*, vol. 115, no. 41, pp. 20153–20159, Oct. 2011.

[72] Tekna, “Induction Plasma Torch PL-35 & PL-50.” 2004.

[73] R. Pristavita, N.-Y. Mendoza-Gonzalez, J.-L. Meunier, and D. Berk, “Carbon Blacks Produced by Thermal Plasma: the Influence of the Reactor Geometry on the Product Morphology,” *Plasma Chem. Plasma Process.*, vol. 30, no. 2, pp. 267–279, Apr. 2010.

[74] R. Pristavita, N.-Y. Mendoza-Gonzalez, J.-L. Meunier, and D. Berk, “Carbon Nanoparticle Production by Inductively Coupled Thermal Plasmas: Controlling the Thermal History of Particle Nucleation,” *Plasma Chem. Plasma Process.*, vol. 31, no. 6, pp. 851–866, Dec. 2011.

[75] “Two-Dimensional Geometry Control of Graphene Nanoflakes Produced by Thermal Plasma for Catalyst Applications | SpringerLink.” [Online]. Available: https://link.springer.com/article/10.1007/s11090-014-9524-6. [Accessed: 04-Feb-2019].

[76] “Platinum(IV) nitrate, solution, Pt 15% w/w - H37737 - Alfa Aesar.” [Online]. Available: https://www.alfa.com/en/catalog/H37737/. [Accessed: 04-Feb-2019].

[77] F. Jaouen, S. Marcotte, J.-P. Dodelet, and G. Lindbergh, “Oxygen Reduction Catalysts for Polymer Electrolyte Fuel Cells from the Pyrolysis of Iron Acetate Adsorbed on Various Carbon Supports,” *J. Phys. Chem. B*, vol. 107, no. 6, pp. 1376–1386, Feb. 2003.

[78] N. Hordy, “Plasma functionalized carbon nanotubes suspensions for high temperature direct absorption thermal energy harvesting,” 2015.

[79] D. B. Holt and D. C. Joy, *SEM Microcharacterization of Semiconductors*. Academic Press, 2013.

[80] D. B. Williams and C. B. Carter, “The Transmission Electron Microscope,” in *Transmission Electron Microscopy*, Springer, Boston, MA, 1996, pp. 3–17.

[81] M. Scimeca, S. Bischetti, H. K. Lamsira, R. Bonfiglio, and E. Bonanno, “Energy Dispersive X-ray (EDX) microanalysis: A powerful tool in biomedical research and diagnosis,” *Eur. J. Histochem. EJH*, vol. 62, no. 1, Mar. 2018.

[82] W. R. Corliss, *Neutron activation analysis*. Oak Ridge, Tenn.: U.S. Atomic Energy Commission, Division of Technical Information, 1963.

[83] J. De Campos, “Synthesis and performance evaluation of a carbon-based catalyst for use in polymer electrolyte membrane fuel cells,” 2018.

[84] “Koutecky-Levich Rotating Disk Electrochemistry (KL-RDE) – Pine Research Instrumentation Store.” [Online]. Available: https://www.pineresearch.com/shop/knowledgebase/pine-aftermath-echem-levich-rde/. [Accessed: 04-Feb-2019].

[85] “Chemical Elements.com - Platinum (Pt).” [Online]. Available: http://www.chemicalelements.com/elements/pt.html. [Accessed: 08-Feb-2019].

[86] "Hydrogen Peroxide Production in the Oxygen Reduction Reaction at Different Electrocatalysts as Quantified by Scanning Electrochemical Microscopy - Analytical Chemistry (ACS Publications)." [Online]. Available: https://pubs.acs.org/doi/10.1021/ac901291v. [Accessed: 19-Feb-2019].

[87] "Determination of the Electron Transfer Number for the Oxygen Reduction Reaction: From Theory to Experiment - ACS Catalysis (ACS Publications)." [Online]. Available: https://pubs.acs.org/doi/10.1021/acscatal.6b01581. [Accessed: 08-Feb-2019].

[88] "Degradation of Perfluorinated Ionomer Membranes for PEM Fuel Cells during Processing with H2O2." [Online]. Available: http://jes.ecsdl.org/content/153/6/A967. [Accessed: 08-Feb-2019].

[89] "20% Platinum on Vulcan XC-72R." [Online]. Available: https://www.fuelcellstore.com/20-platinum-carbon-xc-72r. [Accessed: 03-Feb-2019].

[90] J.-B. Donnet, *Carbon Black: Science and Technology, Second Edition*. Routledge, 2018.